

A Review of Acoustic Liner Experimental Characterization at NASA Langley

*Michael G. Jones, Willie R. Watson, Douglas M. Nark, Brian M. Howerton,
and Martha C. Brown
Langley Research Center, Hampton, Virginia*

NASA STI Program... in Profile

Since its founding, NASA has been dedicated to the advancement of aeronautics and space science. The NASA scientific and technical information (STI) program plays a key part in helping NASA maintain this important role.

The NASA STI Program operates under the auspices of the Agency Chief Information Officer. It collects, organizes, provides for archiving, and disseminates NASA's STI. The NASA STI Program provides access to the NASA Aeronautics and Space Database and its public interface, the NASA Technical Report Server, thus providing one of the largest collections of aeronautical and space science STI in the world. Results are published in both non-NASA channels and by NASA in the NASA STI Report Series, which includes the following report types:

- **TECHNICAL PUBLICATION.** Reports of completed research or a major significant phase of research that present the results of NASA programs and include extensive data or theoretical analysis. Includes compilations of significant scientific and technical data and information deemed to be of continuing reference value. NASA counterpart of peer-reviewed formal professional papers, but having less stringent limitations on manuscript length and extent of graphic presentations.
- **TECHNICAL MEMORANDUM.** Scientific and technical findings that are preliminary or of specialized interest, e.g., quick release reports, working papers, and bibliographies that contain minimal annotation. Does not contain extensive analysis.
- **CONTRACTOR REPORT.** Scientific and technical findings by NASA-sponsored contractors and grantees.

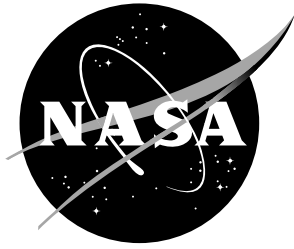
- **CONFERENCE PUBLICATION.** Collected papers from scientific and technical conferences, symposia, seminars, or other meetings sponsored or co-sponsored by NASA.
- **SPECIAL PUBLICATION.** Scientific, technical, or historical information from NASA programs, projects, and missions, often concerned with subjects having substantial public interest.
- **TECHNICAL TRANSLATION.** English-language translations of foreign scientific and technical material pertinent to NASA's mission.

Specialized services also include organizing and publishing research results, distributing specialized research announcements and feeds, providing information desk and personal search support, and enabling data exchange services.

For more information about the NASA STI Program, see the following:

- Access the NASA STI program home page at <http://www.sti.nasa.gov>
- E-mail your question to help@sti.nasa.gov
- Phone the NASA STI Information Desk at 757-864-9658
- Write to:
NASA STI Information Desk
Mail Stop 148
NASA Langley Research Center
Hampton, VA 23681-2199

NASA/TP-2020-220583



A Review of Acoustic Liner Experimental Characterization at NASA Langley

*Michael G. Jones, Willie R. Watson, Douglas M. Nark, Brian M. Howerton,
and Martha C. Brown
Langley Research Center, Hampton, Virginia*

National Aeronautics and
Space Administration

Langley Research Center
Hampton, Virginia 23681-2199

April 2020

Acknowledgments

Special thanks are due to Tony Parrott for his clear and steady guidance during the first three decades of acoustic liner research at the NASA Langley Research Center. Also, the contributions of Carl Gerhold were instrumental in the development of the CDTR. The authors would like to express their appreciation to the many technicians that have contributed to the implementation and usage of the test rigs described in this report. Thanks are also due to Richard Bozak, Matt Galles, Jason June, Jacob Klos, and Frank Simon for their helpful review of this document.

The use of trademarks or names of manufacturers in this report is for accurate reporting and does not constitute an official endorsement, either expressed or implied, of such products or manufacturers by the National Aeronautics and Space Administration.

Available from:

NASA STI Program / Mail Stop 148
NASA Langley Research Center
Hampton, VA 23681-2199
Fax: 757-864-6500

Abstract

This paper presents a review of tools used by the NASA Langley Research Center over the last four decades to experimentally characterize acoustic liners for aircraft noise reduction. Descriptions of past and present NASA test rigs are included to provide context for the application of data acquisition and analysis methods. These test rigs range from simple applications of a raylometer to a waveguide with detailed control over higher-order modes. Methods for impedance eduction based on data acquired in these test rigs are explored in some detail. Strengths and weaknesses of each data acquisition and analysis method are presented, as well as current practices applied in the NASA Langley Liner Technology Facility.

Nomenclature

Symbols	Description
A, B	constants in DC flow resistance equation
A_{mn}, λ_{mn}	mode coefficient and duct eigenvalue of horizontal mode m and vertical mode n
c_p, γ, κ	specific heat at constant pressure, specific heat ratio, heat conduction coefficient
$[C], \{D\}, \{G\}$	Hankel matrix, vector of polynomial coefficients, known right-hand side vector
d_h	hydraulic diameter of duct
f, ω, k	temporal frequency, angular frequency, freespace wavenumber
$F(\zeta), \mathcal{F}(X)$	cost function for eduction, η^{th} degree polynomial for obtaining axial wavenumbers
H, W, h	duct height, duct width, liner core chamber height
i, Γ	unit imaginary number ($\sqrt{-1}$), complex propagation constant
K_{mn}	axial wavenumber for horizontal mode m and vertical mode n
m, n	horizontal (z) and vertical (y) mode orders (written as $\{m, n\}$)
M, U	mean flow Mach number and velocity
N_{mic}	number of microphones
NLF, R_f, \bar{R}	nonlinearity factor, DC flow resistance, DC flow resistivity
p, u, v	acoustic pressure, axial and transverse acoustic particle velocity
$p_{ref}, P_s, \Delta P_s$	reference pressure, static pressure, static pressure drop
P_{mn}	acoustic pressure eigenfunction
\hat{p}_i, \hat{p}_r, R	incident and reflected wave coefficients, reflection coefficient
s, ψ	complex pole, phase angle of complex pole
S, t, ϕ	standing wave ratio, physical time, phase angle
SPL	sound pressure level
t_f	foam thickness
$[U], [V], [\Lambda]$	matrices of left singular vectors, right singular vectors, and singular values
\vec{u}, \vec{n}	acoustic particle velocity vector, unit normal vector into the liner
x, y, z	axial coordinate, vertical coordinate, horizontal coordinate
X, η	zeros and order of polynomial defined in Eq. 36

Symbols	Description
β_v, ν	viscothermal dissipation of acoustic energy, kinematic viscosity
θ, χ, ζ	normalized resistance, normalized reactance, normalized impedance
ρ, c	local density, sound speed of air
ξ	distance from liner surface to first null in standing wave pattern
Φ	phase angle between the facesheet and backplate acoustic pressures
$\ , \bullet$	complex absolute value, vector dot product
Superscripts	Description
$-1, T$	generalized matrix inverse, matrix transpose
$*, \prime$	complex conjugate, ordinary derivative
Subscripts	Description
fs, bp	measurement acquired at facesheet, measurement acquired at backplate
i, r	incident wave component, reflected wave component
j, m, n	counter for acoustic pressure measurements, horizontal and vertical mode orders
num, meas	numerical component, measured component

1 Introduction

Acoustic liners have been studied since the early 1950s for aircraft noise reduction [1]. In general practice, these passive devices are mounted in the walls of an aircraft nacelle inlet and aft-bypass duct to absorb tonal (e.g., noise due to rotor-alone and rotor-stator interaction) and broadband (e.g., noise due to turbulent flow through the nacelle) sources generated by the fan. Liners mounted in current commercial aircraft nacelles (see Fig. 1) are almost exclusively perforate-over-honeycomb structures. They are generally single-degree-of-freedom (SDOF) or double-degree-of-freedom (DDOF) structures, as depicted in Figure 2, in which the DDOF is essentially an SDOF configuration with an embedded porous septum (typically a porous mesh or perforated sheet). Aircraft engine bypass ratio has continually increased to increase propulsive efficiency, with a fortunate byproduct of reduced jet noise. This has caused the broadband fan noise component to become more dominant. As a result, acoustic liners are now needed to absorb sound over a wide frequency range, preferably up to at least two octaves. There has also been a growing interest in the potential for application of acoustic liners on other portions of the aircraft, e.g., on the fuselage or the flap side edge [2, 3]. For these novel applications to be successful, higher-fidelity experimental characterization of these liners is needed.

The NASA Langley Research Center has been conducting acoustic liner research for over four decades. This research can be divided into three main areas of activity: liner modeling, aeroacoustic duct propagation, and experimental characterization of acoustic liners. The last of these is the main focus of this paper. This experimental research has included design and implementation of a number of test rigs to assist in the characterization of acoustic liners. Some of the early test rigs included a raylometer that used a laminar flow meter to achieve controlled air flow, a normal incidence tube

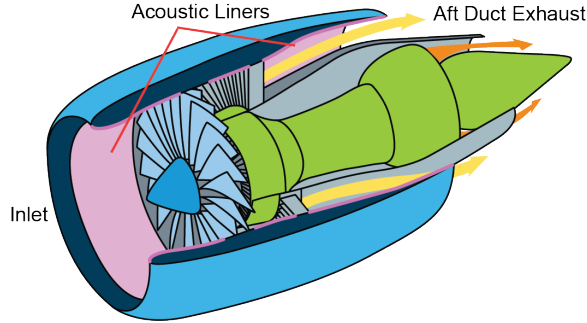


Figure 1: Cutaway sketch of generic aircraft engine nacelle.

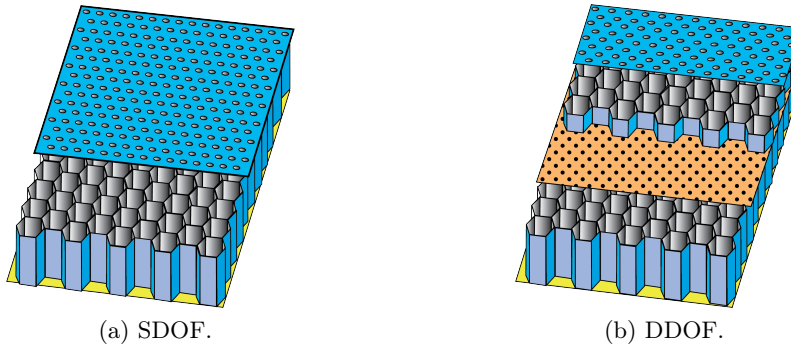


Figure 2: Single (SDOF) and Double (DDOF) degree of freedom acoustic liners.

that employed a traversing microphone probe to measure the incident and reflected sound field, and a flow impedance tube that used a traversing microphone to measure the axially decaying sound field. These test rigs have seen significant enhancement (or replacement) over time. The current test rigs are located in the Liner Technology Facility (see Fig. 3), which is a world-class facility.

This paper is organized in six sections. The following section (Sec. 2) begins with a comparison of the key features of extended-reacting and local-reacting liners. It then provides a description of acoustic impedance, which is the key parameter of interest to the acoustic liner designer, and closes with a brief overview of some of the types of acoustic liners that have been considered at NASA. Section 3 presents an overview of the current NASA Langley test rigs. Section 4 reviews a number of methods used by NASA Langley to characterize acoustic liners, with an emphasis on the determination of acoustic impedance. This section begins with a review of tools that can be used to estimate the acoustic impedance in the limit $f \rightarrow 0$ Hz, and continues with a discussion of methods to evaluate the effects of frequency (f), source sound pressure level (SPL), and source type on acoustic impedance. It closes with a discussion of methods used to account for the effects of grazing flow on the liner impedance. Section 5 presents results used to validate this impedance education process in a more complex acoustic environment. In particular, the effects of higher-order modes are explored. Finally, Section 6 closes with some concluding remarks.

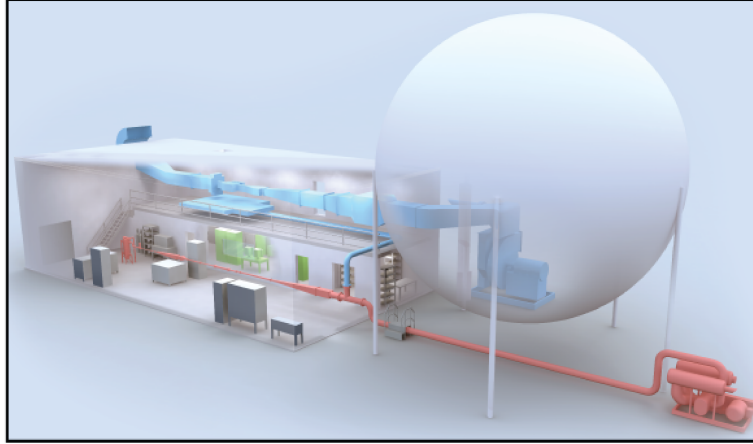


Figure 3: Artist rendering of the NASA Langley Liner Technology Facility. Grazing Flow Impedance Tube (GFIT) and Curved Duct Test Rig (CDTR) are shown in red and blue, respectively.

2 Background

This section presents a brief discussion regarding differences between extended-reacting and local-reacting acoustic liners. It proceeds with an introduction to acoustic impedance, which is an important parameter used to determine the sound absorbing properties of acoustic liners. It then reviews a number of local-reacting and extended-reacting acoustic liner configurations that are, or have been, of interest at NASA.

Extended-Reacting and Local-Reacting Considerations

Acoustic liners are generally classified as ‘extended’ or ‘local’ reaction structures (Fig. 4). One of the most common versions of an extended-reacting liner is one for which the core is filled with foam and there are no (or limited) impervious partitions. The foam may be covered with a perforated facesheet (or perhaps a wire mesh) in order to protect the material from the flow (assuming an aircraft engine nacelle application) over the liner. However, it is also possible to avoid the use of a facesheet if the core material is sufficiently robust (e.g., metallic foam). In either case, the majority of the acoustic resistance is supplied by the foam and sound is transmitted in all directions within the liner. Thus, this type of liner has less resonant behavior (less tonal absorption, as described below) but improved absorption bandwidth relative to conventional local-reacting liners.

Conversely, the local-reacting liner contains impervious partitions that inhibit sound transfer throughout the body of the liner. In general applications (e.g., SDOF and DDOF liners described earlier), the perforate facesheet (or wire mesh) provides enhanced fluid pumping, resulting in spatially concentrated absorption. As a result, this type of liner provides strong absorption over a narrow frequency bandwidth (i.e., good for reduction of tones). As the majority of acoustic liner research is for local-reacting liners, this paper is dedicated to the exploration of different ways to evaluate this type of liner.

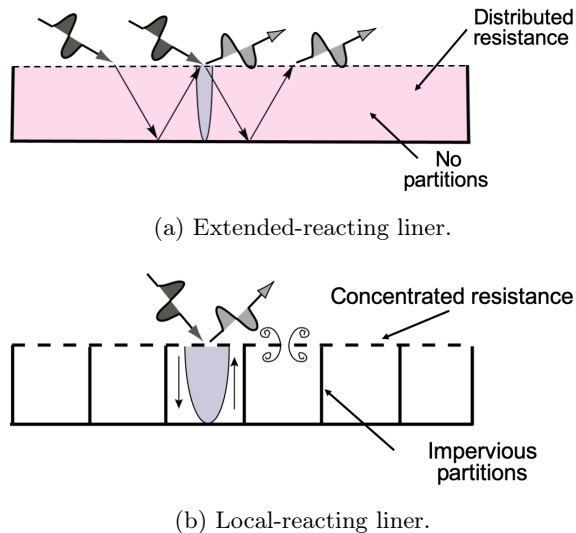


Figure 4: Sketches of extended-reacting and local-reacting liners.

Acoustic Impedance

One of the most important parameters for acoustic liner research is the acoustic impedance. This parameter defines how well the liner will absorb sound under different aeroacoustic conditions. For a local-reacting acoustic liner, it is defined as the ratio of the frequency transforms of the acoustic pressure and the normal component of acoustic particle velocity at a point of interest (e.g., at the surface of the liner) [4]. The acoustic impedance is normalized¹ by the characteristic impedance of air (i.e., ρc) and expressed mathematically by

$$\zeta = \frac{p}{\rho c (\vec{u} \bullet \vec{n})} = \theta + i \chi \quad (1)$$

This impedance is a function of frequency, the liner design and geometry, and the aeroacoustic environment where the liner is placed. Loosely speaking, the resistance is a measure of the forces (e.g., viscous scrubbing losses) that dissipate the acoustic energy (e.g., convert it to heat), while the reactance determines the frequencies for which this energy conversion process is optimal.

For most applications, the sound power absorbed by the acoustic liner is of paramount importance. However, this sound absorption is directly affected by the duct geometry. In contrast, the acoustic impedance is an intrinsic property of an acoustic liner, which implies it is independent of duct geometry. This is critical to the liner designer because it indicates that a detailed study in a controlled environment can be used to determine the acoustic impedance of a liner, and this impedance can then be used to predict the sound absorption of that liner in an aircraft engine nacelle. For example, the NASA Grazing Flow Impedance Tube (GFIT) has been used to determine the impedance of numerous acoustic liners. These impedances are then used to represent acoustic liners via impedance boundary conditions in aeroacoustic duct propagation codes, such that the resultant absorption can be predicted.

¹All impedances are normalized by the characteristic impedance of air, ρc , throughout this paper. For the sake of brevity, the descriptor ‘normalized’ is assumed for the remainder of the narrative.

It is perhaps of interest to note that acoustic impedance typically is not directly measured, as this would require measurements of both the acoustic pressure and the normal component of the acoustic particle velocity (i.e., $\vec{u} \cdot \vec{n}$) at the surface. As our implementation is based solely on the usage of acoustic pressure measurements, this impedance must be inferred or deduced from measurements of other parameters. For this reason, the term ‘eduction’ is often used to convey the manner in which the acoustic impedance is determined.

Acoustic Liners of Interest

Before proceeding with details regarding the evolution of experimental methods used for evaluation of acoustic liners, it is useful to provide a short description of some acoustic liner concepts that are of interest at NASA. Each of these liner concepts is designed with a particular noise reduction goal in mind, which guides the choice of measurement device needed for accurate assessment. This set of liners is chosen simply to provide insight into the breadth of this area of research. Clearly, there are numerous other concepts that are of interest at NASA and throughout the international acoustic liner community.

Figure 2 presents liner configurations that are currently employed in aircraft engine nacelles. Addition of a perforated septum to create a second layer causes the liner to absorb sound over a wider frequency range. Additional degrees of freedom (and thus, increased absorption over the desired frequency range) can be gained by replacing the uniform embedded septum with distinct mesh caps that can be mounted at selected heights and with prescribed resistances in each core chamber (see Fig. 5) [5–10]. One such liner was recently tested on the inlet of a Boeing B737MAX-7 aircraft, and was demonstrated to provide significant noise reduction [11, 12].

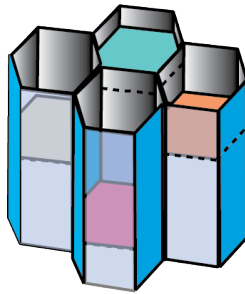


Figure 5: Four chambers of a liner core with embedded mesh caps. Each cap may be at a different height and may have a different resistance.

Another area of interest is the variable-depth liner (see Fig. 6) [5], which is becoming increasingly viable for aircraft applications due to recent advances in additive manufacturing (e.g., 3D printing). As its name implies, the individual core chambers of this liner have different depths, such that each chamber functions as a quarter-wavelength resonator and can thus be tuned to a different frequency. By judicious selection of the different chamber depths (to tune to different frequencies), the liner can be designed to absorb sound over a wide frequency range. The first version (Fig. 6a) employs wide chambers, similar to those of a conventional SDOF liner, and is typically covered with a perforated facesheet. Thus, the majority of the acoustic resistance is achieved via the perforated

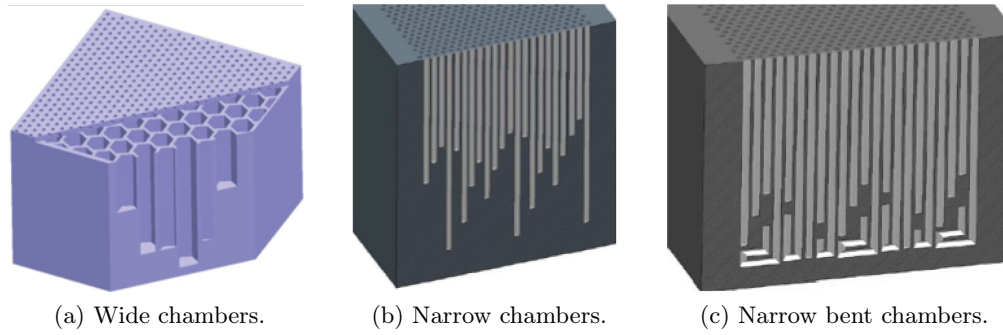


Figure 6: Variable-depth liner configurations.

facesheet. For the other two versions of the concept (Figs. 6b, 6c), the chambers are reduced in diameter. This causes the scrubbing losses along the walls of the chamber to increase significantly, thereby eliminating the requirement of a perforated facesheet. The latter of the two (Fig. 6c) also incorporates bent chambers such that longer chambers can fit into a given volume. This extends the frequency range of absorption to lower frequencies than would be possible with simple SDOF and DDOF configurations.

Foam liners (see Fig. 7) are rarely, if ever, used for aircraft applications because of manufacturing, weight, and durability concerns. However, advances in foam manufacturing suggest that these issues may be solved in the foreseeable future. Metallic foams are becoming more robust and are also able to withstand the issues common to aircraft installations (e.g., exposure to jet fuel, hydraulic fluid, and vibration), but are also more expensive and heavier than conventional liners. Regardless, NASA has considered liners comprised of metallic foam for use in restricted applications (e.g., in the case over the rotor or within flap side edges) [3, 13], because they provide broadband sound absorption. For most of these applications, the metal foam is mounted within core chambers such that the resultant liner is locally reacting.

A common characteristic of most of these liner configurations is that they are designed to achieve increased absorption bandwidth with less volume. Also, these configurations are clearly distinct



Figure 7: Metallic foam liners.

from those that are currently used in aircraft applications. As a result, prediction models must be extended to account for the distinct features of each concept. This requires that the experimental methods used to evaluate these liners be continuously improved such that the results are sufficiently accurate to enable these modeling improvements. Given the nature of these liners, there is also a need for improved experimental and analysis tools to allow more data (due to higher frequency resolution) to be processed quickly.

3 NASA Langley Test Rigs

Over the last four decades, the NASA Langley Research Center has employed a number of test rigs for evaluation of acoustic liners. A photograph of the NASA Langley Liner Technology Facility, which contains each of the current test rigs, is provided in Figure 8. Many of these test rigs have evolved as the instrumentation and hardware options improved, and as new ideas came to light regarding more efficient ways to evaluate acoustic liners. A brief summary of some of the key features for the three acoustics test rigs is provided in Table 1. The remainder of this section reviews current capabilities of the NASA Langley test rigs.

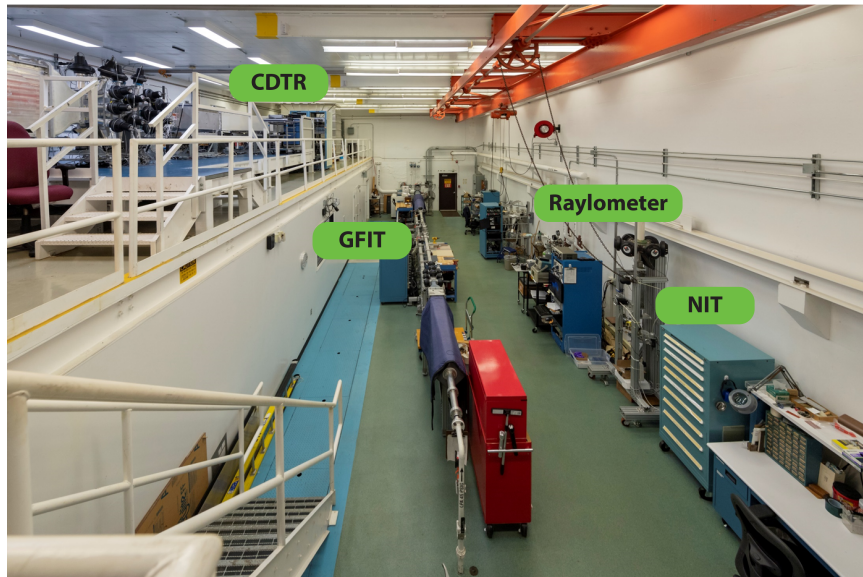


Figure 8: Photograph of the NASA Langley Liner Technology Facility.

3.1 Raylometer

The NASA Raylometer [14] (see Fig. 9) is used to measure the steady or DC flow resistance across a sample, typically the liner facesheet. Metered air is emitted and diffused into the settling chamber. This diffused air passes through a honeycomb mesh to minimize lateral turbulence and three wire

Table 1: NASA Langley Test Rigs - Key Features.

	NIT	GFIT	CDTR
Sample Dimensions			
Length, in (mm)	2 (51)	2 (51)	30 (762)
Width, in (mm)	2 (51)	2 - 24 (51 - 610)	15 (381)
Thickness, in (mm)	≤ 24 (610)	≤ 4 (102)	≤ 3 (76)
Frequency, kHz	0.4 - 3.0	0.4 - 3.0	0.4 - 3.0
Centerline Mach #	0.0	0.0 - 0.6	0.0 - 0.5
Source Type (max level, dB)			
Stepped sine	≤ 155	≤ 155	≤ 140
Swept sine	≤ 145	≤ 145	n/a
Broadband	≤ 140	n/a	≤ 130

mesh screens to reduce axial turbulence. The flow path is then contracted to accelerate the flow, reduce the turbulence, and reduce the boundary layer thickness, such that uniform flow impinges on the surface of the sample.

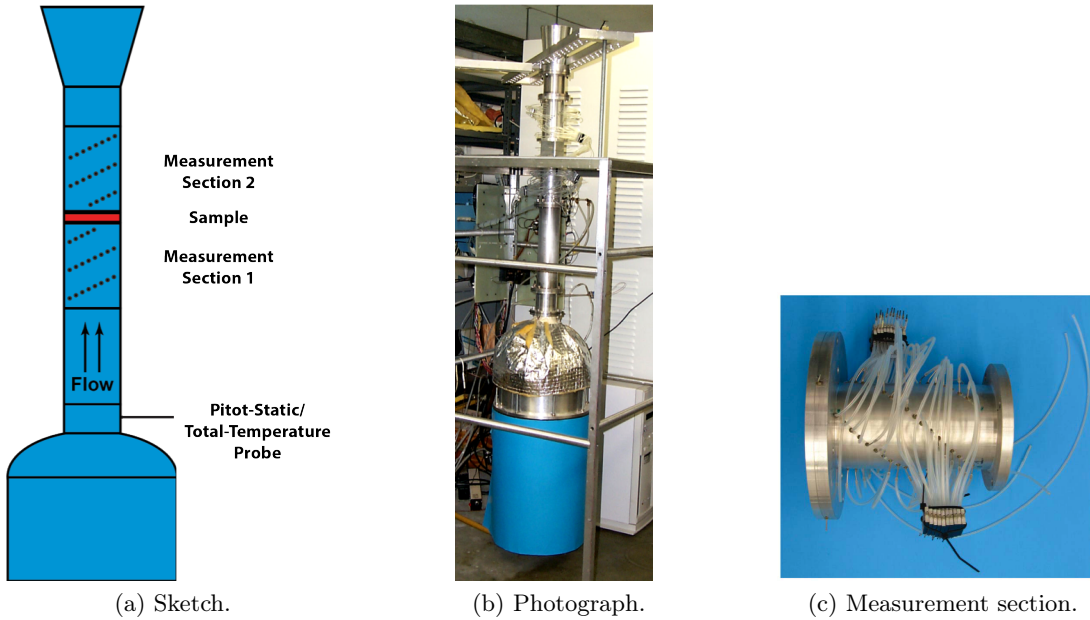


Figure 9: Sketch and photograph with close-up of the NASA Raylometer measurement section.

Next, the flow transitions through a short section of duct containing a pitot-static/total temperature probe used to determine the test flow conditions. This flow then travels through the measurement section upstream of the sample, through the sample itself, and through the mea-

surement section downstream of the sample.² Each of the two measurement sections contains four groups of 20 static pressure ports, mounted in spiral arrays around the duct. By fitting smooth curves (low-order polynomials) to the measured data, any nonuniformities that occur very close to the sample can be taken into account, so that a more accurate estimate of the static pressure drop across the sample can be determined.

A set of five thermal mass flow controllers is used to achieve controlled velocities of 0.2 to 500.0 cm/s. Since the duct area, total pressure and total temperature are known, the average velocity can be determined from the mass flow rate (provided by the mass flow controllers) via application of the conservation of mass law. These mass flow controllers are interconnected via a manifold assembly with solenoid valves, and the entire control system is automated. For quick-look tests, the system is often set to test at three velocities (20, 105, and 200 cm/s). For more detailed investigations, typically as many as ten velocities are used.

3.2 Normal Incidence Tube

Figure 10 provides a photograph of the NASA Normal Incidence Tube (NIT). This device uses six 120 W compression acoustic drivers to produce a sound field that impinges on the surface of the acoustic liner. The 2"×2" waveguide is approximately 36" long, and contains three flush-mounted microphones. A reference microphone located 0.25" from the surface of the liner is typically used to ensure that the liner is exposed to the desired sound pressure level (SPL). Two measurement microphones are positioned 2.50" and 3.75" from the liner surface, and are mounted within a rotating plug such that their positions can be precisely interchanged. This capability is of particular value for the Two-Microphone Method (see Sec. 4.2.4), in that it allows intrinsic amplitude and phase errors due to mismatched calibrations of the two microphones to be eliminated.

The NIT supports three source types: stepped sine, swept sine, and broadband. For the stepped-sine source, measurements are conducted one frequency at a time. The input voltage to a function generator is set to achieve the desired total SPL (within ± 0.5 dB of the target) for the target frequency at the reference microphone. The current system supports testing with total SPLs up to approximately 155 dB, and at frequencies of 0.4 to 3.0 kHz (typically in 0.2 kHz increments). However, tests are typically conducted at two target SPLs (120 and 140 dB) so that the effects of liner nonlinearity on the measured impedance spectra can be explored (this is true for all three source types).

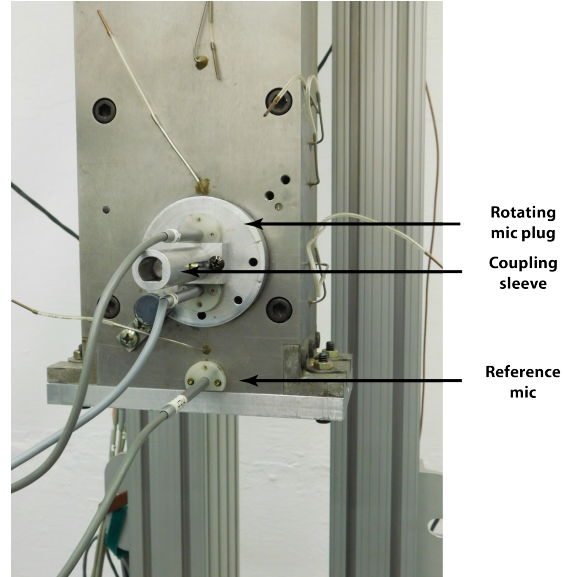
The controlled-amplitude, swept-sine source [15] allows the source amplitude to be maintained to the same accuracy (within ± 0.5 dB of target) while the frequency is swept through the range of interest. This method provides data at approximately 5 Hz increments over the same frequency range, but requires much less time than the stepped-sine approach. However, the maximum SPL that can be currently achieved is approximately 145 dB. Again, tests with this source are commonly conducted at 120 and 140 dB.

The broadband source is based on a white noise electronic signal fed to the six acoustic drivers. For this source, the partial overall SPL measured over the frequency range of 0.4 to 3.0 kHz is set at the reference microphone location, typically at 120 and 140 dB. The full frequency spectra

²Measurement sections are available to support either 2"×2" samples (square duct) or 2"-diameter circular samples (round duct). Also, sheets of material (perforated sheet or wire mesh sheet) can be tested in either configuration.



(a) Photograph of NIT.



(b) Close-up view of measurement section and lower end of waveguide.

Figure 10: NASA Normal Incidence Tube (NIT).

of acoustic pressures at each microphone are then measured simultaneously, and the results are typically reported at 12.5 Hz increments.

3.3 Grazing Flow Impedance Tube

The NASA Langley Grazing Flow Impedance Tube (GFIT, see Fig. 11) has a cross-sectional geometry of 2.0"-wide by 2.5"-high, and allows evaluation of acoustic liners with lengths from 2.0" to 24.0". The surface of the test liner forms a portion of the upper wall of the flow duct (highlighted in blue in Fig. 11). Twelve acoustic drivers form an upstream (exhaust mode) source and six acoustic drivers form a downstream (inlet mode) source. Thus, the operator can choose to operate in either exhaust or inlet mode by choosing which set of acoustic drivers to engage without the need to turn the flow off.

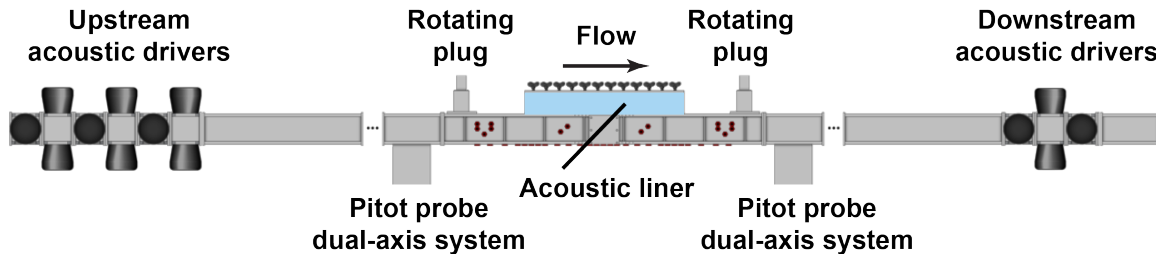


Figure 11: Sketch of the NASA Grazing Flow Impedance Tube (GFIT). Microphones depicted as small cylinders, placed on all walls surrounding the acoustic liner section.

For the last four decades, tests conducted in the GFIT (and its predecessors) have employed the stepped-sine source. In this approach, the acoustic drivers are used to generate tones one frequency at a time over a frequency range of 0.4 to 3.0 kHz, at source SPLs (peak total SPL measured near the leading edge of the liner) up to 155 dB, and at centerline Mach numbers up to 0.6. Voltage to the input function generator is set such that the total SPL at a reference microphone is within ± 0.5 dB of the target value. The location of this reference microphone is discussed in a later section. There are 95 microphones mounted in the rigid walls of the waveguide. Of these, 53 microphones are flush-mounted in the lower wall (opposite the liner) of the GFIT. Acoustic pressures measured with these lower-wall microphones are used for the majority of the analyses described in this report.

Efforts are currently underway to implement the controlled-amplitude, swept-sine source [15] in the GFIT. The description of the swept-sine source provided in Section 3.2 applies for the GFIT as well, with a few exceptions. If the Mach number is held sufficiently low ($M \lesssim 0.2$), then data acquired with sweep lengths (the amount of time over which the signal sweeps through the full frequency range) of 100 to 200 seconds (26 to 52 Hz/s) are acceptable. However, as the grazing flow speed is increased, there is a need to increase the length of the sine sweep to achieve sufficient averaging to suppress the effects of flow noise. Similarly, there is a need to increase the sine sweep length as the source SPL is decreased.

There are a number of topics that are of interest regarding evaluation of acoustic liners with the GFIT. For convenience, some of the more important ones are presented in this section. We begin with a historical review of the transition of flow duct designs beginning around 1980. This is followed with a discussion regarding the methods used to calibrate the array of microphones used in the GFIT. For nonlinear liners, the results are affected by the choice of microphone used to determine the source level. A brief discussion is provided regarding the reasoning for the current choice of reference microphone location. Next, the flow profile traverse systems are discussed. These traverses are used to establish the flow Mach number used in the impedance eduction process.

Over the last decade, there has been much interest in the liner community regarding the effects of flow direction on the impedance eduction process. A brief review of this research topic is provided, along with practical constraints applied in the NASA approach. Clearly, the results achieved with the GFIT are subject to measurement uncertainty. A significant study into these effects on the impedance eduction process was conducted by NASA in the early 2000s. A brief discussion of this study is provided for completeness. Finally, the GFIT has also been used to study the effects of sound on the drag produced by acoustic liners. This measurement process is addressed in the last portion of this section.

Transition of Flow Duct Designs

The original flow duct used by NASA Langley for impedance eduction was the Flow Impedance Tube (FIT). This duct had a 2.0' \times 2.0' cross-section, and was brought online around 1980. The FIT allowed 16"-long liners to be mounted in the lower wall of the test window, and a traversing bar mounted within the upper wall was used to move a flush-mounted microphone over the 33"-long test section [16]. The use of a traversing bar offered two benefits. It allowed the measurements to be spaced differently for each test condition (frequency and Mach number), such that the spatial resolution could be tuned for best results. Since all measurements were made with the same microphone, any calibration concerns were minimal. However, there were problems with the traversing bar. The

traversing bar's dependence on moving parts made it prone to leakage at the interface points (the edges where the sliding bar rubbed against the fixed portion of the duct). Also, movement of the microphone to each measurement location was a slow and tedious process.

In the early 2000s, the FIT was replaced with the Grazing Incidence Tube (GIT) [17]. Three key changes were implemented. First, the traversing bar was replaced with 95 fixed-location microphones. This greatly improved testing efficiency, as multiple microphones could now be read simultaneously. However, this also meant that each microphone needed to be individually calibrated (a laborious task). This latter issue was overcome via development of an in situ calibration process discussed below. The second key change was that the liner was now mounted in the upper wall of the duct. This simplified the mounting process, as gravity held the sample in place while the mounting screws were attached. Finally, the test window was moved well upstream of that used for the FIT, which allowed for evaluation of the effects of developing boundary layer flow.

Around 2010, the Grazing Flow Impedance Tube (GFIT, see Fig. 11) was brought online. A number of enhancements were incorporated into this new design. Some of the more important ones are as follows. First, the cross-section was changed from $2.0'' \times 2.0''$ to $2.5'' \times 2.0''$. Whereas the cut-on frequencies for the first higher-order modes in both the vertical and horizontal dimensions were identical in the square FIT, this change in the vertical dimension caused these modes to cut on at distinct frequencies. This distinction is useful when one is trying to understand results near these cut-on frequencies. Also, the GFIT has acoustic drivers mounted at both ends of the duct, thereby allowing analysis to be conducted in either the exhaust or inlet mode (sound in the same or opposite direction of the flow, respectively). The 95-microphone array of the GIT was adapted with revised microphone locations for implementation in the GFIT. Finally, the GFIT was built using modular components so that the individual sections could be easily interchanged. This allows the test window to be axially moved in one foot increments, which causes the acoustic liner to be exposed to different flow profiles (see Fig. 16) along the length of the duct.

In Situ Microphone Calibration

There are 95 microphones flush-mounted in the walls of the GFIT (see Fig. 12), and the analysis methods presented herein require these microphones (or a subset of them) to accurately record the local acoustic pressures. This requires that each microphone be subjected to an amplitude and phase calibration. The ideal situation is for this calibration to occur immediately prior to the acquisition of research data. It is also useful to conduct a post-test calibration to ensure no changes to the response functions occurred during the test, especially if the test is lengthy. Fortunately, the intrinsic properties of these microphones are such that their amplitude and phase response are virtually frequency independent.

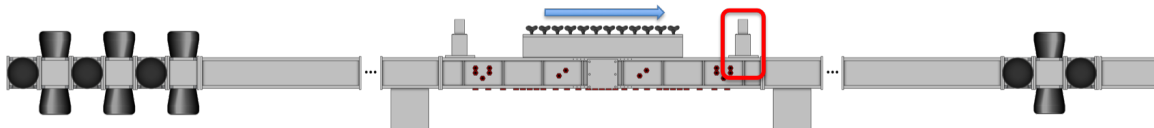


Figure 12: Grazing Flow Impedance Tube with downstream rotating plug highlighted.

Given the number of microphones, the calibration process would be quite lengthy with an external calibrator, in which each microphone must be individually mounted in the calibrator for evaluation. Instead, an in situ microphone calibration process is used. The highlighted section (red box in Fig. 12) indicates the location of a rotating plug that contains two microphones flush-mounted in the upper wall, upstream of where the liner would typically be located. This rotating plug allows the locations of these two microphones to be precisely interchanged, thereby allowing for implementation of the Two-Microphone Method (TMM, see Sec. 4.2.4). The calibration process is performed as follows:

1. Remove one of the microphones from the rotating plug and use an external calibrator to calibrate this microphone. Reinstall this microphone into the rotating plug.
2. Install a hardwall insert (where the test liner would normally be mounted) to ensure all of the walls of the duct are rigid (with embedded microphones).
3. With the flow turned off (Mach 0.0), use the upstream array of acoustic drivers to engage a single-tone source at a selected frequency and a total SPL (measured with the rotating-plug microphone that was calibrated in step 1) of 120 dB. The frequency must be well below the cut-on frequency of the first higher-order mode, and the choice of SPL is selected to ensure the sound field is linear. This tone will propagate through the GFIT and will be reflected at the downstream array of acoustic drivers and the duct termination. This combination of forward and backward sound waves sets up a standing wave pattern in the test section (portion of the duct containing the microphones) that can be evaluated using the TMM.
4. Use the acoustic pressures measured with the two microphones within the rotating plug as input to the TMM to determine the impedance of the downstream section of the duct. This impedance is then used to compute the standing wave pattern throughout the test section.
5. Use the standing wave pattern to compute the SPL and phase that should be present at each microphone location in the duct.
6. Apply calibration corrections to each microphone such that they produce these expected readings. As a side note, a need for significant correction suggests the possibility of a failing microphone.
7. Conduct steps 3 - 5 with a second frequency. The calibration process is deemed successful if the predicted and measured values for the SPL and phase are matched to within an acceptable tolerance. (Note: When this step has been performed successfully on multiple occasions, it is replaced with a comparison of new calibration factors against those used in recent tests, to ensure there are no issues with a particular microphone, signal conditioner, or analog-to-digital acquisition device.)

The selection of the initial frequency is important. Ideally, this frequency is chosen such that the standing wave is suitable for the process. If the termination is nearly anechoic for the selected frequency, the TMM process becomes exceedingly sensitive because both microphones are exposed to nearly identical SPLs. On the other hand, if the termination is highly reflective, there is the possibility that a null in the standing wave pattern will exist at one of the microphone locations. Again, this causes difficulties to the TMM. Nevertheless, it is generally not too difficult to find a

frequency that provides an acceptable standing wave ratio (preferably on the order of 5 dB). Strictly speaking, this calibration process is capable of providing accurate results to within ± 0.01 dB and $\pm 0.1^\circ$. However, when the system effects (mounting sample, setting flow conditions, etc.) are included, the acoustic pressures measured in the GFIT have been determined to be accurate to within ± 0.5 dB and $\pm 1.0^\circ$.

Reference Microphone Location

The majority of the NASA methods are initiated by setting the total (sum of the incident and reflected waves) SPL at a reference microphone. The choice of location for this reference microphone can have a noticeable impact on the impedance reduction results. Two choices have been used in the GFIT and its predecessors (see Fig. 13). There are pros and cons for each of these options.

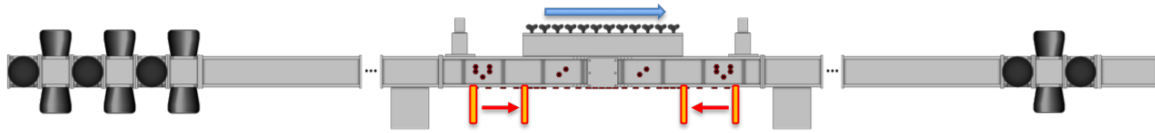


Figure 13: Grazing Flow Impedance Tube with transitions of reference microphones shown in red for inlet and aft modes of operation.

The first option is to place the reference microphone 8" upstream of the leading edge of the liner. This distance from the liner is sufficient to ensure that evanescent modes generated at the impedance discontinuity at the leading edge of the liner should die out before reaching the axial plane of the reference microphone. However, reflections from this impedance discontinuity cause a standing wave in the hardwall region upstream of the liner. For those frequencies where the standing wave ratio is small (reflections are minimal), these reflections cause no great difficulties. At frequencies where this standing wave ratio becomes significant, a null in the pattern may occur at the reference microphone location. Indeed, this is found to occur at frequencies near 1.2 kHz. As a result, if the source level setting algorithm is designed to ensure a constant level at the reference microphone, this means the SPL at the liner leading edge will be significantly different. Figure 14 presents axial acoustic pressure profiles in the GFIT measured for frequencies of 1.0 and 1.2 kHz. Although the levels at the reference microphone (located at $x = 0.0$ " for this measurement) are within 0.1 dB for the two frequencies, they diverge by approximately 4 dB at the leading edge of the liner (at $x = 8.0$ "). If the liner is linear (i.e., impedance is insensitive to changes in SPL), this is not important. However, for nonlinear liners, this is problematic.

A second option is to place the reference microphone at or near the edge of the liner that is closest to the source (leading edge for exhaust mode, trailing edge for inlet mode), where the peak acoustic pressure amplitude occurs. Because of the difficulties noted above, this is currently the preferred approach. Due to impedance discontinuities and the possible presence of evanescent modes at the edge of the liner, this peak amplitude may be slightly displaced from the edge of the liner. Therefore, a search routine is employed to select the microphone within ± 3 " of the edge of the liner that measures the highest amplitude. This microphone is then used as the reference microphone

(location of the reference microphone may change with frequency). This ensures that all frequencies are tested with very nearly the same SPL entering the treated section.

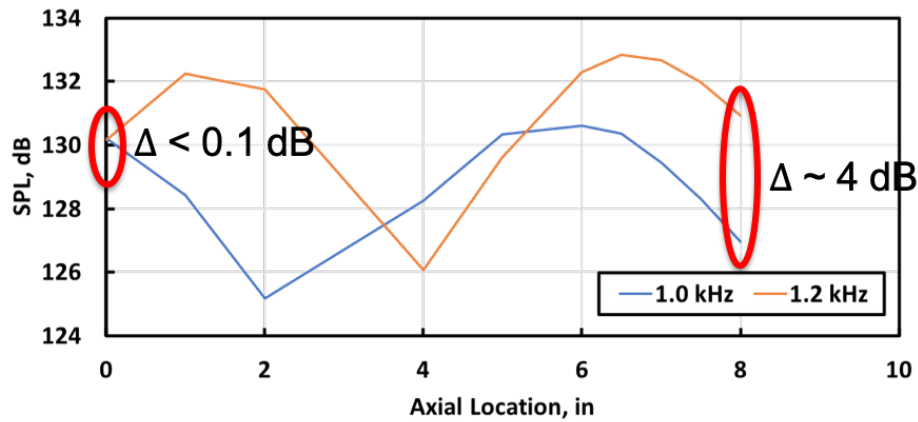


Figure 14: Effects of changes in reference microphone location.

Flow Profile Traverse Systems

As noted earlier, the GFIT is built using a modular approach, such that individual components can be interchanged. One of these components is a traverse system consisting of a pitot probe (total pressure probe with a flattened tip suitable for near-wall boundary layer measurements) that is positioned via a two-directional stepper motor system. This system allows the total pressure to be measured across a single axial plane approximately 8" upstream of the source plane (see Fig. 15) when the duct is operated in the exhaust mode.

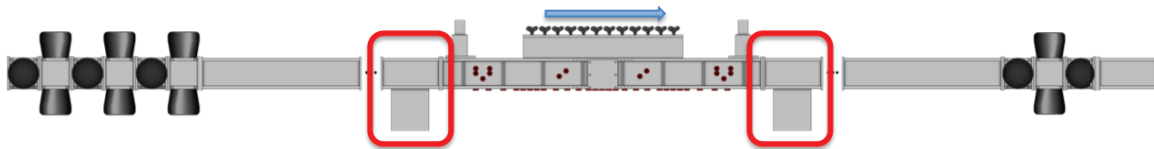


Figure 15: Grazing Flow Impedance Tube with two flow profile traverse systems enclosed in red boxes.

A static pressure port is positioned in the same axial plane as the measurement port of the pitot tube, such that their respective readings can be combined with the total temperature of the duct (measured at duct centerline, approximately 10' downstream of the axial midpoint of the acoustic liner) as input to the isentropic equation to determine the flow velocity. Typically, the total pressure is measured at 279 locations organized in a 9×31 (9 horizontal, 31 vertical) array. Note that these calculations assume the total temperature to be conserved over this 10' length of duct, and any

deviations in the total temperature will cause the computed Mach number to be in error. The wall temperature (measured via a separate thermocouple) is used to achieve a near-adiabatic wall condition, so any such errors should be minimal. However, given the importance of very small changes in the average Mach number used in the impedance eduction analysis, an acoustics-based approach is preferred (see the next section) for the determination of the average Mach number.

The impedance eduction methods discussed herein are also based on the assumption of parallel flow, i.e., the flow profile is assumed to be invariant over the length of the test section. In reality, the flow through the duct is Fanno flow, i.e., the centerline flow accelerates (see Fig. 16) along the length of the duct (it will choke if the duct is sufficiently long). Nevertheless, the variability between the two flow profiles upstream and downstream of the liner is not large. Thus, the flow profile used in the impedance eduction analyses is typically based on a weighted average of flow profile measurements conducted at two axial locations, one upstream of the test section and another just downstream of the test section. The weighting is based on the distance from each traverse to the axial midpoint of the liner, which changes based on the liner length. For the second (downstream) acquisition, the traverse system previously needed to be moved to the downstream location. This meant the flow had to be turned off, the traverse system moved, and the flow brought back online at the same conditions. This was a time-consuming operation. Fortunately, as indicated in Figure 15, a second traverse has recently been added, thereby greatly increasing the efficiency of the flow profile data acquisition. It should be noted that the pitot probes are retracted into the wall when acoustic data are being acquired such that they do not impact acoustic measurements.

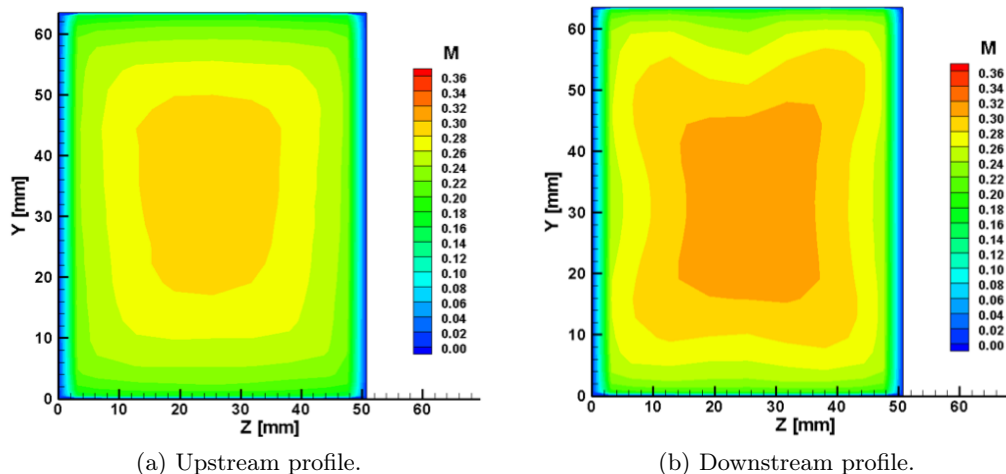


Figure 16: Flow profiles measured upstream and downstream of the GFIT test section; setpoint centerline Mach number of 0.3.

Flow Direction Effects on Impedance Eduction Process

Over the last decade, there has been significant interest in the liner community regarding the effects of flow direction on the impedance eduction process. It has long been accepted that the acoustic

impedance should be independent of the flow direction. However, until recently, most test facilities tended to operate in the exhaust mode (flow and sound in the same direction) and this assumption was therefore rarely tested.

In 2011, Renou et al. [18] observed differences between impedance spectra deduced for an SDOF liner when the source was moved from upstream (exhaust mode) to downstream (inlet mode) of the liner. Their proposal was to replace the Myers boundary condition with a modified version empirically derived to account for these differences. Also in 2011, Eversman et al. [19] proposed including the uniform flow Mach number as an optimization parameter in the impedance eduction process for the exhaust mode, but did not apply this approach to inlet mode data at that time. The following year, Watson et al. [20] presented results for multiple liners tested in the GFIT. They also proposed an approach based on data acquired in both the exhaust and inlet modes, but found that this approach produced anomalies at the highest Mach number of interest (Mach 0.5). They suggested that this was likely due to a need to include shear flow effects in the analysis, and also observed that impedance eduction using the inlet mode was more sensitive to slight errors than those using the exhaust mode.

In 2014, Zhou et al. [21] presented comparisons of impedance eduction results for a single liner tested in multiple test rigs. Their results suggested the local Mach number just outside the viscous wall region could be used with the Myers boundary condition to bring the exhaust and inlet mode impedance spectra into better agreement. The next year, Zhou et al. [22] used results of an uncertainty analysis to suggest a local Mach number based on friction velocity might be a better choice. Their results showed convergence between the exhaust and inlet mode impedance spectra at lower frequencies (below the resonance of the liner, where the effects of the cavity are dominant), but the results diverged at higher frequencies (above resonance, where the effects of the perforated plate become more important). In 2017, Schulz et al. [23] suggested the momentum transfer impedance (i.e., ratio of shear stress and normal particle velocity at the wall) can be used with the duct wall's normal incidence impedance to properly categorize the acoustic boundary condition.

In 2018, Nark et al. [24] presented results based on a combination of linear and nonlinear liners tested in the GFIT using the configuration shown in Figure 17. They showed that a very minor adjustment ($\Delta M \leq 0.02$) to the estimate of the average Mach number caused the impedance spectra deduced in the exhaust and inlet modes to coalesce quite well (see Fig. 18). This correction was shown to work for a number of distinct liner configurations, i.e., it is not liner dependent. Finally, in 2019, Roncen et al. [25] explored the possibility that the differences in impedance were due to shear flow effects, but found that this was insufficient to explain all of the differences.

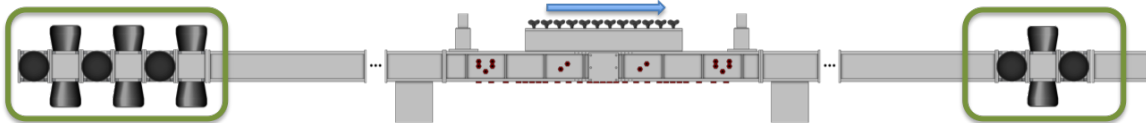
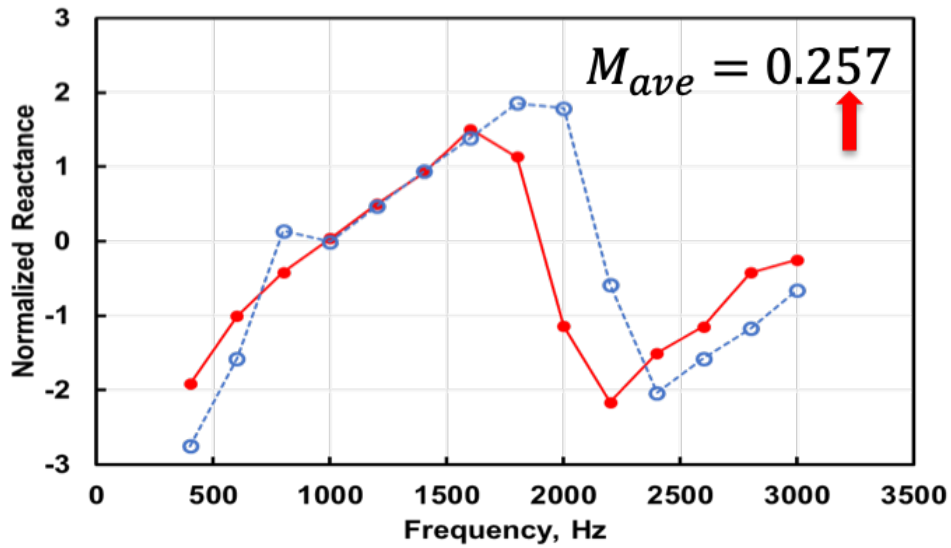
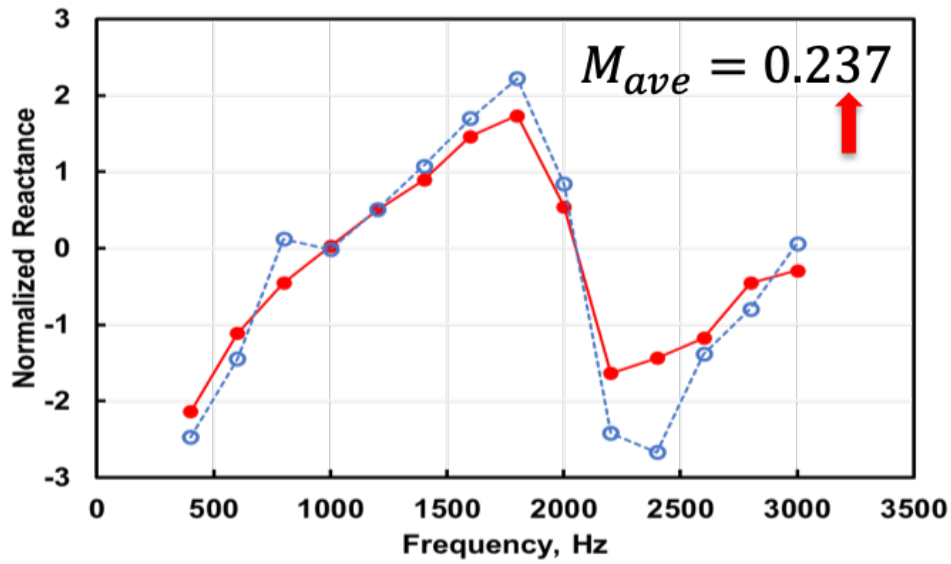


Figure 17: Grazing Flow Impedance Tube with two source sections shown in green boxes.



(a) Uncorrected results.



(b) Corrected results.

Figure 18: Effects of minor Mach number corrections (change from 0.257 to 0.237) on acoustic reactance spectra. Results for the upstream (exhaust mode) and downstream (inlet mode) source locations are represented with red solid and blue dashed lines, respectively.

It is the view of the authors that each of these viewpoints has merit, especially when one is seeking to learn all they can about a particular liner configuration. Nevertheless, the Myers boundary condition remains as the boundary condition of choice for liner analysis conducted at NASA.

First, it should be recalled that an average Mach number is based on a number of measurements conducted at multiple axial locations in the GFIT. It is therefore quite reasonable to accept that the estimated average (averaged over the cross-sectional area) Mach number could be in error by 0.02 (the adjustment proposed by Nark). Second, it should be noted that the ‘final’ application for most of our research is intended to be the implementation of a liner in the walls of an aircraft engine nacelle. For that application, detailed flow field information is rarely provided. Instead, average Mach numbers are typically provided at one or two axial locations within the nacelle. While it is useful to include the shear flow effects [26], it is also important to maintain consistency between the method used to reduce the impedance and the propagation calculation that is used to predict the results for the final application. Hence, if a uniform-flow assumption is to be used in the final propagation calculation, then it is imperative that the impedance to be used as a boundary condition should also be reduced using a uniform-flow assumption.

This investigation into the effects of flow direction on the impedance reduction process has proven very useful. Now that the corrected average Mach number has been determined based on the assumption that the impedance of the liner should be flow direction independent, it is convenient to limit the majority of our tests to the exhaust mode. This is useful, as data acquisition in the GFIT is more robust for the exhaust mode. Specifically, the upstream source section is capable of providing higher source SPLs and the sensitivity to slight changes in the flow is lower.

Measurement Uncertainty

An overarching concern for experimental characterization of acoustic liners is the uncertainty of the parameters used in this characterization. In the early 2000s, NASA conducted a lengthy assessment study [27] to determine appropriate uncertainty bounds (to include systematic and random uncertainty) for each of the parameters used for impedance reduction in the presence of flow (see Sec. 4.3). This study was conducted using the GIT (predecessor to the current flow duct, GFIT). A single conventional liner (perforate over honeycomb) was tested approximately 10 times for each test condition (6 frequencies, 3 Mach numbers, 2 source SPLs) over the course of about 18 months, so that effects due to weather changes could be captured. The sample was removed and reinstalled in the GIT for each repeat test, so that the effects of liner mounting were also measured. The results were used to compute 95% confidence intervals for a number of geometric and aeroacoustic parameters.³ Because of the similarity between the GIT and GFIT, those uncertainties are used as a guide for the majority of the work currently conducted in the GFIT.⁴

Liner Drag

Interest in liner drag has grown over the last decade. As the cost of jet fuel continues to rise, there is increasing interest in reducing the drag due to acoustic liners. Also, increases in the turbofan diameter have increased the total liner area while decreasing the duct length to diameter ratio, such that small improvements in liner drag can have a large impact. It has therefore become important to develop liners that maximize the acoustic absorption while minimizing the drag. There are many facilities that are suitable for measuring the drag due to the roughness of the liner surface, typically

³Note that the labels for the last two columns of Tables 6.2 and 6.3 in that report [27] should be reversed.

⁴Another portion of this assessment study [28] was devoted to a description of aeroacoustic propagation codes used at NASA. The effects of measurement uncertainty on the resultant propagation results were also addressed as part of the assessment.

with the aid of a force balance. As demonstrated by Howerton et al. [29–31], the GFIT can also be used for this purpose. This method is based on a precise measurement of the static pressure drop over the length of the liner (see Fig. 19). Of particular note is the fact that the GFIT can be used to explore the interactive effects of acoustics and liner drag. It has been demonstrated that the liner drag is increased by the addition of sound when that sound is of sufficiently high amplitude [29, 30, 32]. As an example, if a conventional liner is exposed to Mach 0.3 grazing flow, the liner drag is relatively constant if the source SPL is held below approximately 140 dB, but increases for higher source SPL. Similarly, if the flow is increased to Mach 0.5, the liner drag remains constant if the source SPL is held below approximately 150 dB.

Alterations to the geometry of facesheet perforations have been shown to have an effect on liner drag, both positively and negatively. Thus, it is important, and now possible, to perform trade-off studies of aerodynamic performance (liner drag) against acoustic performance (noise reduction).

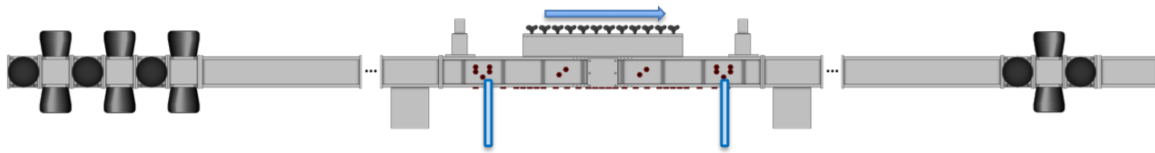


Figure 19: Grazing Flow Impedance Tube with locations of static pressure ports for use in drag estimation highlighted in blue.

3.4 Curved Duct Test Rig

The NASA Curved Duct Test Rig (CDTR) [33,34] is designed to assess the acoustic and aerodynamic performance of aircraft engine nacelle liners (Fig. 20). The CDTR has a cross-sectional geometry of 6”-wide by 15”-high. The test section size is therefore between 100% and 25% of the scale of the aft bypass ducts of aircraft engines ranging in size from business jet to large passenger jet. The CDTR is an open-loop wind tunnel that uses a fan to draw unconditioned atmospheric (outdoor) air through the test section. It can be operated with three test window configurations. The most common configuration is a straight duct, as depicted in Figure 21a. Two curved configurations are occasionally used (which is the basis for the name of the test rig) [35], where the test window outlet is offset from the inlet by 3” or 6”. The latter is depicted in Figure 21b. Acoustic liners can be mounted in either (or both) of the sidewalls of the CDTR (see Fig. 21).

Similar to the GFIT, the CDTR can be operated in both exhaust and inlet modes. However, the transition process for doing so is much more complicated in the CDTR. The array of acoustic drivers is mounted on wheels such that it can be positioned at either side of the test window. Switching from one mode to the other involves rewiring of the associated cabling for the microphones and acoustic drivers. This process typically requires about one day.

Sound is generated in the test section of the CDTR by an array of 31 acoustic drivers. Three source types are commonly used: stepped sine with controlled modes (can control up to 15 modes in each direction), stepped sine with uncontrolled modes, and broadband. For the stepped-sine sources, the source is tonal and is applied one frequency at a time. For the broadband source, a

white noise signal is used. Regardless of the source type, tests are typically conducted over the frequency range of 0.4 to 3.0 kHz.



Figure 20: Photograph of the Curved Duct Test Rig (CDTR).

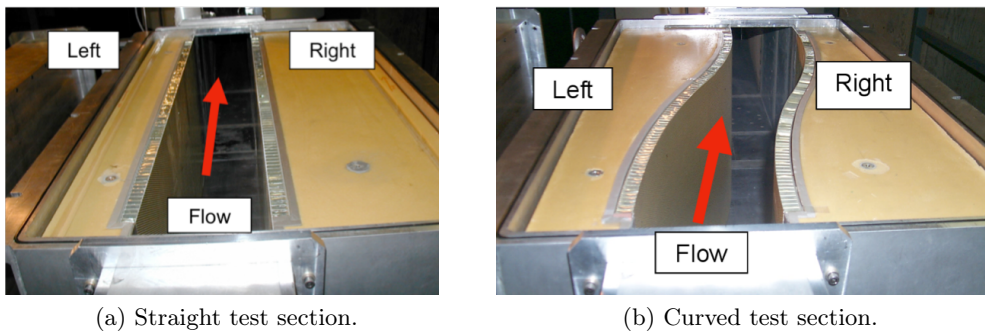


Figure 21: Photographs of straight and curved test sections.

For the controlled-mode, stepped-sine source, the amplitude and phase of the desired tone (one frequency at a time) is independently set at each driver such that a desired higher-order mode can be achieved. The array of 63 microphones (flush-mounted in the hardwall section upstream of the liner) is used to provide feedback to ensure the target mode has the desired amplitude while the

other modes are suppressed. The maximum tonal sound level that can be generated in the duct is on the order of 140 dB, with the amplitude of the desired mode typically at least 10 dB above the amplitude of all other modes. For the other two sources, the voltage to each acoustic driver is typically set to the maximum level such that the overall SPL in the duct is maximized.

Arrays of 63 microphones upstream and downstream of the 15"×30" liners (liners mounted in one or both sidewalls) are used to decompose the sound fields into higher-order modes. Thus, comparison of the upstream and downstream modal content allows one to determine the absorptive capability of the liner for each mode. In addition, 32 microphones are mounted in the upper wall of the flow path when the straight configuration is used. These microphones are used to monitor the sound field within the treated section (the portion containing the liner), and can be used with the Prony method (see Sec. 4.3.5) to deduce the liner impedance in the presence of higher-order modes.

Microphone Calibration

Due to the large CDTR flow path cross-section, the in situ calibration process employed in the GFIT is not suitable for the CDTR. Also, the microphones currently used in the CDTR have a frequency-dependent response. Thus, each microphone must be tested in an external amplitude and phase calibrator, for multiple SPLs and frequencies (from 0.125 to 4.000 kHz). After the microphones have been placed back into the CDTR, sound is generated at 130 dB and 0.35 kHz (only plane waves can propagate at this low frequency) and the SPL and relative phase are measured by each microphone. A comparison of these measured data with those acquired in previous tests is used as a quality check to ensure that the system is behaving as expected.

This calibration process is much more time-consuming (typically, two to three days) than the one used for the GFIT. Immediately after the calibration is completed, the estimated uncertainty is similar to that attained in the GFIT. However, as this calibration process cannot be conducted as often, there is some concern regarding gradual degradation as time elapses from when the most recent calibration was completed. The existing microphones are gradually being replaced with higher quality microphones similar to those used in the GFIT. The response of these replacement microphones is frequency independent, such that calibration at a single frequency can be confidently used over the entire frequency range. This means it should be possible to perform an in situ calibration process similar to that employed in the GFIT, and to therefore significantly reduce the time required for the calibration process.

Flow Profile Traverse Systems

The CDTR has a two-directional traverse system similar to that used in the GFIT. This system allows the total pressure to be measured across a single axial plane approximately 8" upstream of the leading edge of the liner. Again, a static pressure port is positioned in the same axial plane as the measurement port of the pitot tube, such that their respective readings can be combined with the total temperature of the duct (measured in a low velocity section well upstream of the test window) as input to the isentropic equation to determine the flow velocity.

The CDTR has multiple test window configurations. One test window contains four one-directional traverse systems used to measure the flow profile at four axial locations distributed over the length of the treated section [36]. These flow profiles are used to determine the momentum thickness of the boundary layer flow at these locations. The momentum loss over the length of the liner is used to estimate the drag due to the roughness and acoustic response of the liner.

4 Acoustic Impedance Determination

This section presents a brief review of a number of methods used to characterize acoustic liners at various levels of fidelity. It begins with discussion of the DC flow resistance of the liner facesheet, which is determined with the use of a raylometer. This is followed by a review of different methods to assess the response of the liner when it is exposed to a sound field. Specifically, the effects of frequency, source SPL, and source type (tonal or broadband) on the measured impedance are explored.

Next, methods used to include the additional effects of grazing flow on the acoustic impedance are explored. Most of the methods presented herein are based on an assumption that the source sound field is comprised solely of plane waves. This is generally sufficient, as the acoustic impedance is independent of the source modal content. However, the sound field in the aircraft engine nacelle contains numerous higher-order modes, and it is therefore of interest to understand the effects of the acoustic liner on a sound field including these modes. These effects are briefly explored in the final section of this paper.

4.1 DC Flow Resistance

One of the more basic test rigs for liner evaluation is the raylometer. This test rig is often used to evaluate the liner facesheet, typically either a wire mesh or a perforated sheet. Specifically, the raylometer is used to measure the DC flow resistance of the facesheet, which can be used as an estimate of the acoustic resistance in the limit $f \rightarrow 0$ Hz [27]. For many liners, the acoustic resistance is relatively independent of frequency. Thus, the raylometer serves as a useful tool for the liner designer.

In its most simple form, the raylometer consists of two sections of pipe with flanges that allow a sample (in our case, the liner facesheet) to be mounted between them. A laminar flow element is mounted in the upstream section of pipe to measure the flow velocity through the sample, and static pressure ports are positioned upstream and downstream of the sample (see Fig. 22). These ports must be positioned sufficiently far from the liner component to avoid issues caused by nonuniform liner components. In other words, the measurements must be made sufficiently far from the surface such that the static pressure is uniform across the duct. The NASA Langley Raylometer (see Fig. 9) represents an extension of this simple concept, where automated mass flow controllers are used to set the mean velocity through the sample, and spiral arrays of static pressure ports are used to more accurately determine the static pressure drop across the sample.



Figure 22: Sketch of basic raylometer.

The DC flow resistance, R_f , is computed as

$$R_f = \frac{\Delta P_s}{U}. \quad (2)$$

When this DC flow resistance is normalized by the characteristic impedance of air, ρc , the resultant quantity provides a good estimate of the acoustic resistance in the limit $f \rightarrow 0$ Hz.

These data are typically measured at flow velocities of 20, 105, and 200 cm/s. The value measured at 105 cm/s is labeled as the DC flow resistance, R_f , of the material. The other two values are used to compute the nonlinearity factor, NLF, given by

$$\text{NLF} = \frac{R_f |_{200 \text{ cm/s}}}{R_f |_{20 \text{ cm/s}}}. \quad (3)$$

Wire mesh facesheets are of interest because of their very low nonlinearity. To give an idea of the order of magnitude, the NLF for most wire meshes used in aircraft applications tends to be less than two. For evaluation of acoustic liners, the velocities of greatest interest are typically those that correspond to the acoustic particle velocities expected in the acoustic application (in this case, the aircraft engine nacelle). Thus, since the acoustic particle velocity increases with increasing SPL, this low NLF indicates that an acoustic liner with a wire mesh facesheet will be very insensitive to changes in the SPL. This ‘linearizing’ feature allows for improved control of the liner impedance when exposed to a variety of sound fields, thereby aiding in the modeling of the expected absorption results.

By contrast, conventional perforates generally are much more nonlinear, with NLFs up to approximately 10. As such, they are generally more sensitive to changes in the acoustic particle velocity (and therefore the source SPL). This makes the task of designing the liner more difficult, as the sound field varies significantly within the aircraft engine nacelle. Indeed, if the acoustic liner is performing well, the resultant sound absorption causes the liners near the end of the duct (inlet for forward radiating noise, fan exhaust for backward radiating noise) to experience a lower SPL than those near the fan. Regardless, the raylometer can be used to quickly compare different facesheets to determine which is likely to be most suitable for the chosen application.

Although this test approach is quite simple, it can be used for more complicated test environments. One such implementation was presented by Syed, et al., in 2002 [37], in which the liner component was in the wall of a larger flow duct. This allowed measurement of the DC flow resistance across the liner component while it was exposed to grazing flows similar to those experienced in a turbofan engine. In addition, this approach supported evaluation of the effects of a sound field (in the main duct) on the liner component.

It is often of interest to more thoroughly evaluate the effects of velocity on the DC flow resistance through the perforate facesheet. This resistance can be broken into linear and nonlinear contributions, given by

$$R_f = A + BU, \quad (4)$$

where the constants A and B are determined by fitting the equation to data acquired over the velocity range of interest. In practice, accurate determination of the A constant requires measurements at very low velocities. Unfortunately, most raylometers are sensitive to slight changes in the atmospheric pressure. Hence, it is critical that this type of measurement be made under very stable atmospheric conditions. As noted earlier (see Sec. 3.1), the NASA Raylometer employs multiple static pressure ports and thermal mass flow controllers to mitigate these issues.

Another use for the raylometer is to evaluate the properties of foams, specifically the flow resistivity. This flow resistivity, \bar{R} , is given by

$$\bar{R} = \frac{R_f}{t_f}. \quad (5)$$

Of particular interest at NASA is the usage of metallic foams [3, 13]. For many applications, the optimum normalized resistance for an acoustic liner is unity. Thus, a simple measurement of a representative thickness of foam can be used (via Eq. (5)) to determine the appropriate thickness needed to achieve this optimum.

4.2 Effects of Frequency, Source Sound Pressure Level, and Source Type

Whereas the raylometer is used to study the liner facesheet, the NIT shown in Figure 23 can be used to gain insight into the effects of frequency, source SPL, and source type (tonal or broadband) on the acoustic impedance of the full liner (facesheet, honeycomb core, and backplate). Sound is emitted from an acoustic source through a waveguide to impinge on the surface of an acoustic liner mounted to the termination. A portion of the sound is absorbed by the liner, and the remainder is reflected into the waveguide. This combination of forward and backward traveling waves combines to set up a standing wave pattern.

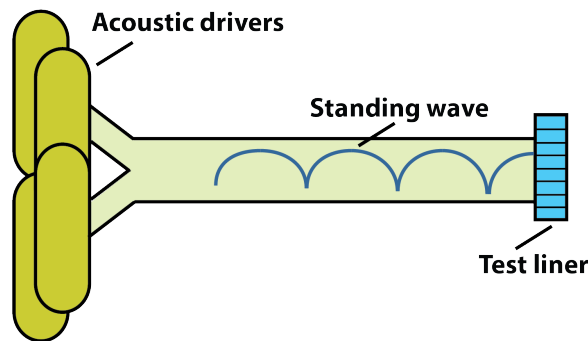


Figure 23: Sketch of normal incidence tube (NIT).

An acoustic liner is labeled as ‘linear’ if its acoustic impedance is completely insensitive to changes in the acoustic particle velocity and, therefore, to changes in the SPL at the surface of the liner. As such, the NLF of the facesheet for a linear acoustic liner is unity. Thus, liners with a wire mesh facesheet are generally very linear.

When a perforated facesheet is employed, the linearity of the liner is strongly influenced by the facesheet thickness-to-hole diameter ratio. Specifically, nonlinear effects lessen (i.e., the liner becomes more linear and NLF of the facesheet decreases) as this ratio increases. Conventional, perforate-over-honeycomb liners, with facesheet thickness-to-hole diameter ratios close to unity, are generally found to be weakly nonlinear at frequencies away from resonance (frequency where the reactance experiences a positive-slope zero crossing), and much more nonlinear near resonance. As

a result, their acoustic impedance is a function of the SPL at the surface of the liner. For nonlinear liners, it is therefore critical to ensure that the surface SPL is set to the desired value.

There are two commonly used options for setting the source SPL. Some researchers prefer to set the incident SPL, while others prefer to set the total (sum of incident and reflected) SPL. There are many reasons for this difference of preference, but the most common one is related to the manner in which the resultant data is to be used. If the results are to be used with a duct propagation code, then it is of value to set the source SPL in the measurement in a manner that will be consistent with the way in which the source is input in the code. Since the acoustic liner responds to the total SPL that is present at the liner surface, most tests conducted in the NASA test rigs (as well as most analyses conducted using NASA propagation codes) use the total SPL as a setpoint.

Both tonal and broadband sound are present in the engine nacelle. Although the differences are generally not large, the effects of source type on the acoustic impedance are clearly present. For example, the acoustic resistance is dependent on the rms (root-mean-squared) acoustic particle velocity [38], which is related to the overall sound pressure level (OASPL) measured over the full frequency range of the sound field to which the liner is exposed. As such, a thorough evaluation of an acoustic liner includes studies with both tonal and broadband sources.

An example of the difference between results acquired using tonal and broadband sources is shown in Figures 24 - 26. Impedance spectra were deduced using the Two-Microphone Method (see Sec. 4.2.4) with data acquired in the NIT. The test sample was a conventional perforate-over-honeycomb liner. Four tests were conducted, two with a tonal source, and two with a broadband noise source. The tonal tests were conducted with source SPLs of 120 and 140 dB, and the broadband noise tests were conducted at OASPLs of 120 and 140 dB.

The resistance spectra depict significant effects of the source SPL and source type. The effects of source SPL are demonstrated by comparison of the two broadband results, where the resistance spectrum for the 140 dB source is 0.2 to 0.3 higher than the corresponding spectrum for the 120 dB source. An increase in resistance is also observed for a tonal source. However, this effect is clearly frequency dependent, with larger increases near resonance. The effects of source type are negligible in the reactance spectra, while increases in source SPL cause the reactance spectra to become slightly flatter (reduced frequency dependence). This flattening of the reactance spectra causes the absorption coefficient spectra to broaden with increasing source SPL. This feature has been further explored by Simon et al [39]. They used a Lattice Boltzmann analysis to study the frequency dependence of the impedance spectrum when the source SPL is increased. Interestingly, they also found that if the level is increased high enough (170 dB in their study), the flattening of the reactance spectrum causes the resultant absorption spectrum to also become much less frequency dependent for nonlinear liners.

The SPL at an individual narrow band frequency is approximately 20 dB below the total OASPL for the dataset presented in Figures 24 - 26. In other words, when the OASPL is set to 120 dB, the SPL at an individual frequency is approximately 100 dB. This means that the SPL at a single frequency is either 120 dB or 140 dB for the two tonal sources, and is either 100 dB or 120 dB for the two broadband sources. Therefore, if the resistance is solely dependent on the acoustic particle velocity at an individual frequency, the results for the 120 dB tonal source should match those for the 140 dB OASPL broadband source. On the other hand, if the resistance is dependent on the rms acoustic particle velocity, as is indicated in many impedance prediction models [40], the tonal results should match those for the 120 dB OASPL broadband source.

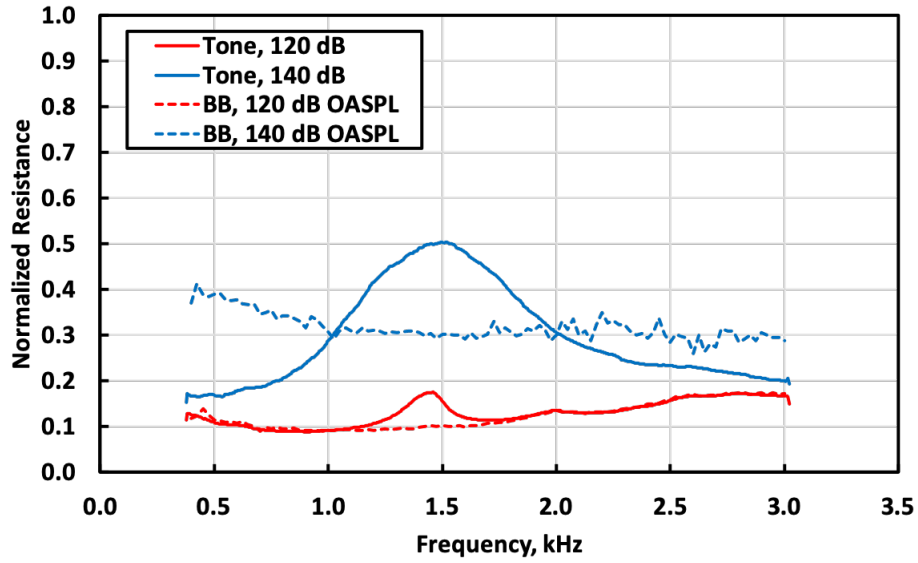


Figure 24: Comparison of resistance spectra for two source types and two SPLs.

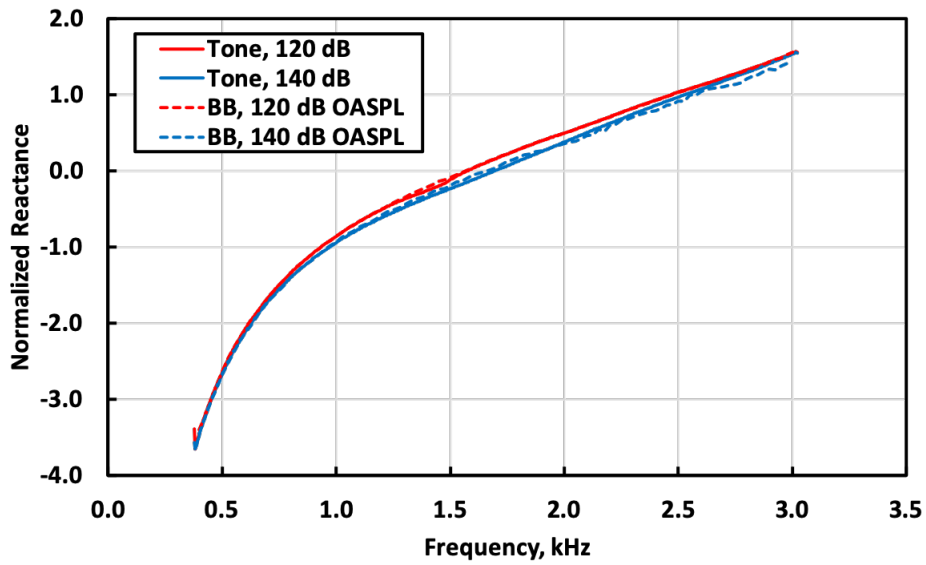


Figure 25: Comparison of reactance spectra for two source types and two SPLs.

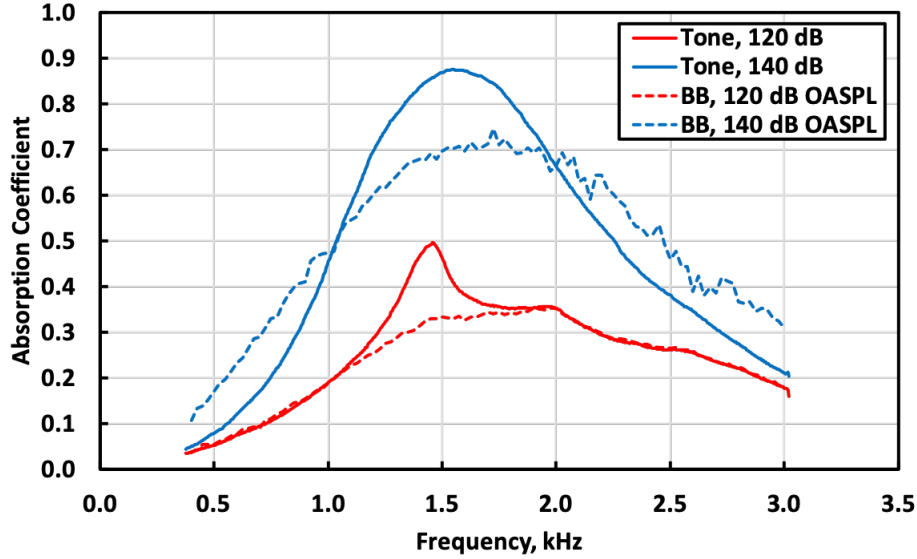


Figure 26: Comparison of absorption coefficient spectra for two source types and two SPLs.

As shown in Figure 24, the resistance spectrum for the 120 dB tonal source compares favorably to that for the 120 dB broadband source, except for frequencies near resonance. In this frequency regime, the resistance is higher for the tonal source than for the broadband source. The same is not true at 140 dB. The resistance peak near resonance for the tonal source is much stronger than that observed for the 120 dB source. Also, the resistance spectrum for the broadband source is relatively frequency independent, with a value that is nominally an average of the range of values measured with the tonal source.

The favorable comparison for the 120 dB tonal and 120 dB broadband sources partially validates the assumption that the liner responds to the rms acoustic particle velocity rather than simply to the acoustic particle velocity at an individual frequency. Perhaps more important to the current review, it clearly demonstrates that the effects of source SPL and source type must be taken into account for a thorough evaluation of an acoustic liner.

Regardless of the source type, the measured acoustic pressures are processed via discrete Fourier transforms to separate the results according to frequency. The analysis provided below is conducted in the frequency domain. Thus, the use of broadband data simply requires this analysis to be performed on a frequency by frequency basis.

There are multiple approaches that have been considered for evaluation of the resultant sound field in order to determine the acoustic impedance of the liner. The remainder of this section provides a brief description of some of the approaches that have been employed at NASA. Equations provided with each method represent the analysis approaches that were employed when these methods were being heavily used. In most cases, these derivations were driven by the instrumentation and computational tools that were available at the time.

4.2.1 In Situ Method (ISM)

In the early 1970s, Dean [41] presented the In Situ Method (ISM) for determination of the liner impedance. This method typically employs microphones flush mounted in the facesheet and backplate of the liner, as shown in Figure 27. The impedance of the liner can be computed as

$$\zeta = \frac{p_{fs}}{\rho c u_{fs}} = \frac{-ie^{i\Phi}}{\sin(kh)} \frac{p_{fs}}{p_{bp}}. \quad (6)$$

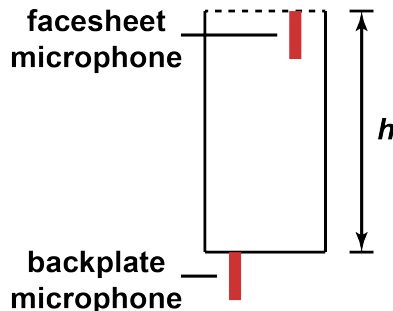


Figure 27: Sketch of liner with microphones mounted in facesheet and backplate for use in the In Situ Method (ISM).

One very attractive feature of this method is that it can not only be applied in a laboratory (e.g., for a liner mounted in the NIT or GFIT), but can also be applied in an aircraft engine nacelle. By comparison, it is very difficult (or often impossible) to apply many of the other methods presented in this report to liners mounted in the walls of an engine nacelle. For the case of no flow (engine off), the impedance can be measured via a ‘plunker’, which is a portable NIT. However, if the engine is powered on, the options for evaluation of the in situ acoustic properties for liners mounted in engine nacelles become very limited. Thus, in large part because of the fact that the ISM can be applied for liners in an engine nacelle, this method continues to be used [42–44].

Since the microphones are mounted directly into the liner, there are some resultant issues. Of particular note is the fact that the measurement microphones replace a portion of the liner that is to be evaluated, i.e., it is an invasive method. Also, this method provides a local impedance, i.e., the results are directly affected by the local aeroacoustic environment. To account for this fact, users often mount multiple pairs of microphones at different locations throughout the liner to attain an estimate of the global impedance (i.e., an impedance that represents the entirety of the liner). Regardless, this local versus global comparison must be incorporated into the final assessment of results achieved using this method.

It is important to pay attention to the effects of microphone positioning [44]. The facesheet microphone should be mounted outside the hydrodynamic near field of the perforate, a constraint that is often difficult to achieve depending on the choice of perforate hole diameter and facesheet porosity. Similarly, the effects of backplate microphone positioning must be considered, as the results can be different if this microphone is mounted near the center of the chamber instead of

near the edge. Also, since the facesheet microphone will typically be inserted through one chamber of the liner, the body of the microphone causes blockage in that chamber. These blockage effects should be taken into account in the analysis. Finally, it is important to ensure proper sealing around the edges of the microphones, as leakage effects will distort the results. Although others have had success with the ISM, the aforementioned difficulties have resulted in limited usage at NASA.

4.2.2 Standing Wave Method (SWM)

One of the earlier methods used to evaluate acoustic liners with the NIT was the Standing Wave Method [45]. The NASA implementation used a 3'-long probe that could be traversed via stepper motor control to measure the acoustic pressure along the axial extent of the NIT (see Fig. 28). This probe had an opening in the wall to allow sound to enter at one end, and a microphone connected to the other end was used to record the acoustic pressure.

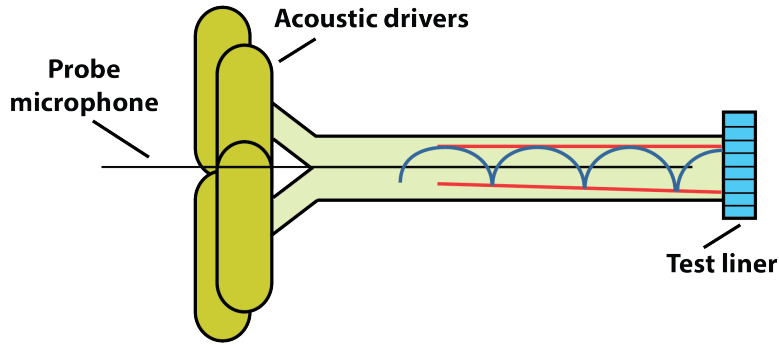


Figure 28: Sketch of NIT with probe microphone for use in Standing Wave Method (SWM).

Figure 29 provides an expanded view of a standing wave pattern in the NIT. The acoustic pressure, p , in the waveguide is given by

$$p = p_i e^{i(\omega t - kx)} + p_r e^{i(\omega t + kx)} \quad (7)$$

where x represents the axial distance from the surface of the sample. The standing wave pattern created by the combination of the incident and reflected waves has a nearly constant peak pressure. However, the SPL at the nulls increases with increasing distance from the surface of the sample. As a result, the standing wave ratio (difference between peak and null of the standing wave pattern) gradually decreases with increasing distance from the sample (e.g., $S_0 > S_1 > S_2 > S_3$ in Fig. 29).

If one fits straight lines to the peak pressures and the null pressures (red lines in Figs. 28 and 29), these curve-fits can be extrapolated to the surface of the liner to estimate the standing wave ratio at the surface of the sample, S_0 . When this standing wave ratio and the distance from the sample to the first null, ξ , are known, one can then compute the acoustic impedance of the liner as [46, 47]

$$\zeta = \frac{1 + \Psi e^{i\Theta}}{1 - \Psi e^{i\Theta}} \quad (8)$$

where Ψ is the ratio of pressure magnitudes

$$\Psi = \frac{\|p_r\|}{\|p_i\|} = \frac{10^{S_0/20} - 1}{10^{S_0/20} + 1} \quad (9)$$

and

$$\Theta = -\pi - 2k\xi. \quad (10)$$

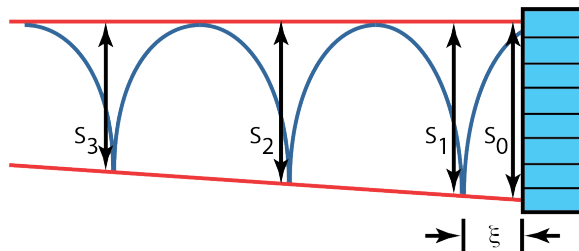


Figure 29: Sketch of standing wave with key parameters.

A few items are worth noting regarding this method. It assumes that only plane waves are present in the waveguide, and thus limits the frequency range of applicability. For example, the first higher-order mode cuts on in the NASA Langley NIT at around 3400 Hz. The method is also quite time consuming, as it requires the precise determination of multiple peaks and nulls in the standing wave pattern. This is achieved by carefully traversing the probe microphone while measuring the acoustic pressure at each axial location. In practice, a number of search algorithms have been considered to improve the efficiency of this measurement. Another option is to use the first standing wave ratio (S_1 in Fig. 29) as an estimate of the true standing wave ratio, S_0 , to reduce the acquisition time. Nevertheless, this remains a tedious process.

If the acoustic liner is a very poor absorber (approaching a hardwall condition), the standing wave ratio can become quite large, and the nulls that occur every half-wavelength become very narrow. In this case, it becomes quite difficult to accurately determine the SPL at a null, as this measurement requires very precise positioning and also requires that the measurement port be sufficiently small to resolve the measurement. In other words, it is critical that the measurement port be sufficiently small that when the pressure field is averaged over the surface of that port, it remains representative of the true null value at the center of the port. Since the SPL varies very little over a small axial extent for locations near the peak, the size of the measurement port becomes less critical for measurements in that region.

Note that the SWM can be used with limited instrumentation. The acoustic pressure magnitude is directly proportional to the AC voltage measured via the microphone mounted to the end of the measurement probe. Thus, the SWM can be conducted with a voltmeter and any method suitable for determining the location of the measurement port. Indeed, one of the initial approaches was to use a hand-controlled positioning device while monitoring the microphone output on an analog voltmeter (a very tedious process)! The process became much easier when computers were implemented with a stepping motor to control the positioning of the probe and the analog voltmeter was replaced with a digital voltmeter.

In summary, the SWM has experienced wide usage and offers a direct method for determining the effects of frequency and source SPL on the acoustic impedance of a test liner. Regardless, since this method is time-consuming, it is now rarely used by NASA.

4.2.3 Multipoint Method (MPM)

In the late 1980s, NASA developed the Multipoint Method (MPM) [48,49] to replace the SWM. By this time, computers and discrete Fourier transform data acquisition devices had become commonplace in most laboratories, and each of these was useful in this replacement method. The MPM was conducted with the same probe system as was used with the SWM, but required much less input data to determine the liner impedance.

If the acoustic pressure field in the waveguide (NIT) is confined to plane waves, it can be described by

$$p_j = [p_i e^{-i\Gamma x_j} + p_r e^{i\Gamma x_j}] e^{i\omega t} \quad (11)$$

where Γ is defined as

$$\Gamma = k + i\beta_v \quad (12)$$

and the viscothermal dissipation of acoustic energy at the wall of the NIT, β_v , is given by [50]

$$\beta_v = \frac{\sqrt{2}k}{d_h} \left[\sqrt{\frac{\nu}{\omega}} + (\gamma - 1) \sqrt{\frac{\kappa/c_p}{\rho\omega}} \right]. \quad (13)$$

All of the parameters used in Equation (11) are assumed known except for the incident and reflected acoustic pressures, p_i and p_r . Thus, these two parameters could be determined from measurements at two axial locations (two equations and two unknowns). Instead, the MPM is based on measurements of the acoustic pressure at multiple axial locations, and the incident and reflected acoustic pressures are determined via a least-squares fit to the measured data. In practice, optimum results (best accuracy for a given amount of acquisition time) are achieved with six measurements acquired within the first half-wavelength from the liner surface. If the incident and reflected acoustic pressures are known, the acoustic impedance is given by

$$\zeta = \frac{1 + R}{1 - R}; \text{ where } R = \frac{p_r}{p_i}. \quad (14)$$

As noted above, this method assumes that only plane waves are present in the waveguide, thereby limiting the frequency range of applicability. However, the useful frequency range can be extended by use of a specialized probe (see Fig. 30) that consists of four hollow tubes protruding from the main stem. Each protrusion contains a measurement port at the null of the first higher-order mode. In this manner, sound received at each of the four evenly distributed ports is merged to provide an averaged acoustic pressure at the face of the microphone mounted at the end of the main stem of the measurement probe. This process is intended to average out any discrepancies introduced if the ports are not precisely located at the null locations. With this process, the effects of the first higher-order mode in both directions are negligible, thereby allowing plane-wave analysis to be used to much higher frequencies.

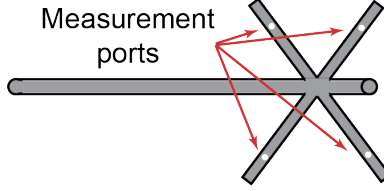


Figure 30: Sketch of specialized probe.

Since this method only requires six measurements at predetermined, frequency-dependent locations, it provides a significant reduction in data acquisition time relative to the SWM. As with the SWM, this method does not require detailed microphone calibrations since the same microphone is used for all measurements. The MPM remains in use for those cases where the Two-Microphone Method is not suitable (see Sec. 4.2.4). For these cases, the measurements previously acquired with the probe microphone are now acquired with multiple microphones flush-mounted in the wall of the waveguide.

4.2.4 Two-Microphone Method (TMM)

A detailed study [49] was conducted by NASA in the late 1990s to compare results for multiple methods to measure liner impedance using the NIT. This study included the SWM and MPM described above, as well as the Two-Microphone Method (TMM) [51]. The main difference between the TMM and the MPM is the restriction to only use acoustic pressures measured at two prescribed distances from the liner surface. Whereas the MPM uses a least-squares fit to multiple (in our case, six) measurements to solve Equations (11) - (14), the TMM solves them in a deterministic manner (two equations and two unknowns).

Initially, the TMM was implemented with the probe system used in the SWM and MPM. However, the TMM is more commonly conducted using two fixed-location microphones. As shown in Figure 31, two measurement microphones are flush-mounted in the wall of the NIT. Typically, the two acoustic pressures are measured simultaneously, thereby greatly reducing the time required.

The two measurement microphones must be accurately calibrated to properly account for any differences in their response. However, this requirement may be mitigated by use of the switching method. In the NASA implementation, a stepper motor is used to precisely interchange the locations of the two microphones, which are flush-mounted within a rotating plug. In this implementation, the acoustic pressures are measured with the two microphones in one orientation, the plug is rotated, and the acoustic pressures are measured again with the microphone locations in the reverse orientation. The results from the two sets of readings are geometrically averaged, taking into account the respective orientations, to determine the true acoustic pressures at each location.

While the TMM is much more efficient than the SWM or MPM, it introduces a few other issues. For those frequencies where the two microphones are positioned one half-wavelength apart, the acoustic pressures at both locations are nearly identical. In this case, the results are more sensitive to slight errors in the measurements. As such, the microphone calibration process becomes even more critical at these frequencies. Also, if the TMM is implemented with flush-mounted microphones, as used in the NASA approach, the value that is measured by a microphone is a weighted average of the acoustic pressure over the entirety of its surface. This averaging process causes the results to be slightly less accurate. Nevertheless, due to the efficiency of this approach, it remains as the main

analysis method used by NASA for analysis of NIT data.

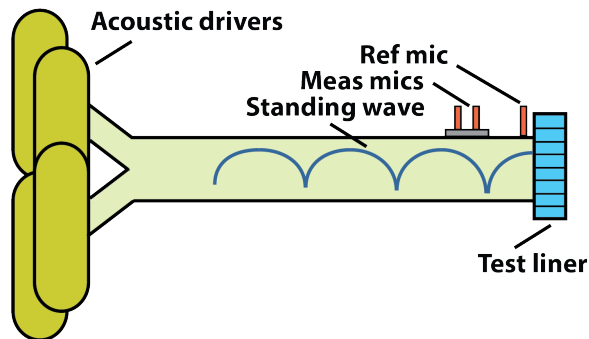


Figure 31: Sketch of NIT with microphone setup for use with Two-Microphone Method (TMM).

4.3 Additional Effects of Grazing Flow

Acoustic liners mounted in the walls of an aircraft engine nacelle are exposed to a complex sound field. The rotating fan and the resultant rotating flow field interacting with the fan exit guide vanes (also called stator vanes) generate tones [52]. The interaction of turbulent flow with the rotor and fan exit guide vanes also generates broadband noise. Thus, the acoustic liner is exposed to tones, broadband noise, and grazing flow. The addition of grazing flow significantly increases the difficulty of determining the acoustic impedance of liners. This topic has been of significant interest to the liner community for at least four decades, and is a major focus of the research conducted by the NASA Langley Liner Physics Team.

The methods used to determine the acoustic impedance can be classified as direct or indirect. Direct methods use measurements of the aeroacoustic environment to compute the impedance directly, while the indirect methods combine these measurements with a duct propagation code to reduce the liner impedance. Some of the direct and indirect methods employed at NASA are discussed in the remainder of this section. Each of these methods reduces the impedance based on data acquired with the NASA Langley GFIT.

4.3.1 Methods Based on the Convected Helmholtz Equation (CHE and PyCHE)

The first method to be presented employs a finite element solution to the convected Helmholtz equation (CHE). This method has been a mainstay of NASA Langley acoustic liner research for at least three decades, and continues to be regularly used today. It assumes the flow is uniform and the sound fields upstream ($0 \leq x \leq x_1$) and downstream ($x_2 \leq x \leq L$) of the liner (see Fig. 32) contain no higher-order modes. Under these assumptions, the acoustic field satisfies a convected Helmholtz equation on the acoustic pressure fields (assuming a time dependence of the form $e^{i\omega t}$)

$$(1 - M^2) \frac{\partial^2 p(x, y)}{\partial x^2} + \frac{\partial^2 p(x, y)}{\partial y^2} - 2ikM \frac{\partial p(x, y)}{\partial x} + k^2 p(x, y) = 0. \quad (15)$$

The local-reacting wall boundary condition presented by Myers [53] is given by

$$-\frac{\partial p(x, H)}{\partial y} = ik \left(\frac{p(x, H)}{\zeta} \right) + 2M \frac{\partial}{\partial x} \left(\frac{p(x, H)}{\zeta} \right) + \frac{M^2}{ik} \frac{\partial^2}{\partial x^2} \left(\frac{p(x, H)}{\zeta} \right), \quad (16)$$

where the normalized admittance, $1/\zeta$, is taken as zero along the rigid wall portion of the upper wall and H is the duct height (2.5" for the GFIT). As a side note, other versions of the liner boundary condition have been considered [18, 20, 54], but none have provided noticeable improvement to the results achieved with GFIT data.

The normal component of the acoustic particle velocity vanishes at the rigid lower wall

$$\frac{\partial p(x, 0)}{\partial y} = 0, \quad (17)$$

and the acoustic pressures at the source and exit planes are assumed known from measurements on the lower wall

$$p(0, y) = p(0, 0); \quad p(L, y) = p(L, 0). \quad (18)$$

If the acoustic impedance of the liner is known, Equations (15) - (18) may be solved via a finite element method to determine the acoustic pressure field throughout the GFIT. The CHE method employs an optimizer to search for an impedance where the acoustic pressures predicted via this finite element method match the corresponding acoustic pressures measured with the microphones along the lower wall of the GFIT to within an acceptable tolerance. This is achieved by minimizing the cost function

$$F(\zeta) = \sum_{j=1}^{N_{mic}} \|p(x_j, 0)_{num} - p(x_j, 0)_{meas}\| \quad (19)$$

where N_{mic} is the number of microphones in the lower wall (53 for the GFIT).

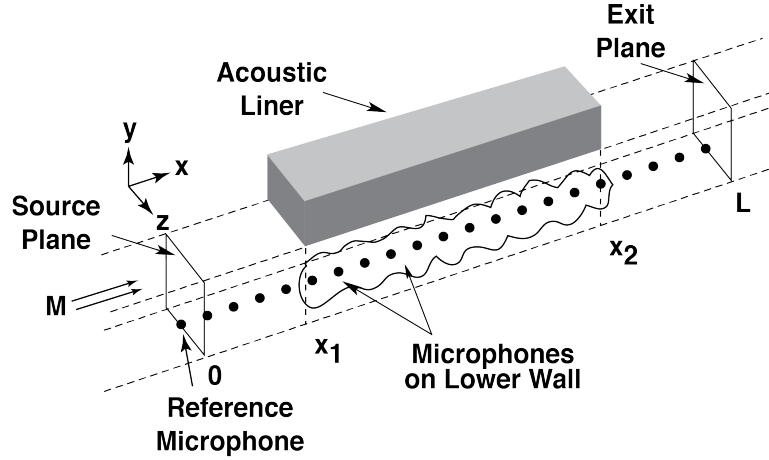


Figure 32: Sketch of computational domain in GFIT.

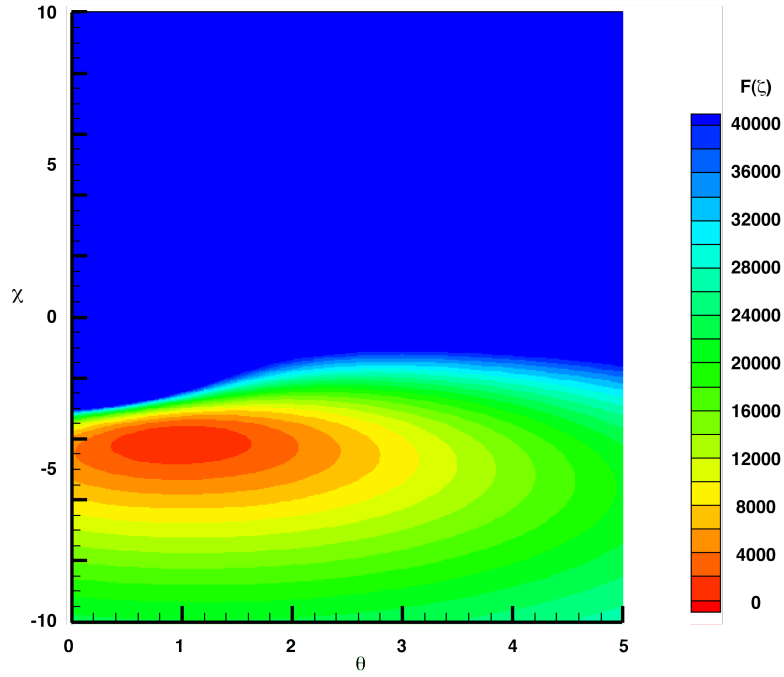
The CHE method has been in use at the NASA Langley Research Center for a number of years. For much of that time, Stewart's adaptation of the Davidon-Fletcher-Powell (SDFP) optimization

algorithm [55, 56] was employed to minimize the cost function, $F(\zeta)$. The SDFP is a gradient-based optimizer, and is therefore subject to the possibility of finding local minima for the cost function. To circumvent this issue, four separate optimizations are typically conducted for each test condition with distinct initial estimates for the liner impedance. These four initial estimates are $0.5 + 0.5i$, $0.5 - 0.5i$, $2.0 + 0.5i$, and $2.0 - 0.5i$. The four resultant educed impedances are then compared to determine the ‘correct’ impedance. Typically, these results are identical, i.e., each optimization has converged to the global optimum. If this is not the case, the anomalous results must be resolved via ‘engineering judgment.’ Fortunately, the impedance spectrum for a uniform liner is generally a smooth function, so the anomalous results will be clearly evident; i.e., they will appear as discontinuities in the impedance spectrum.

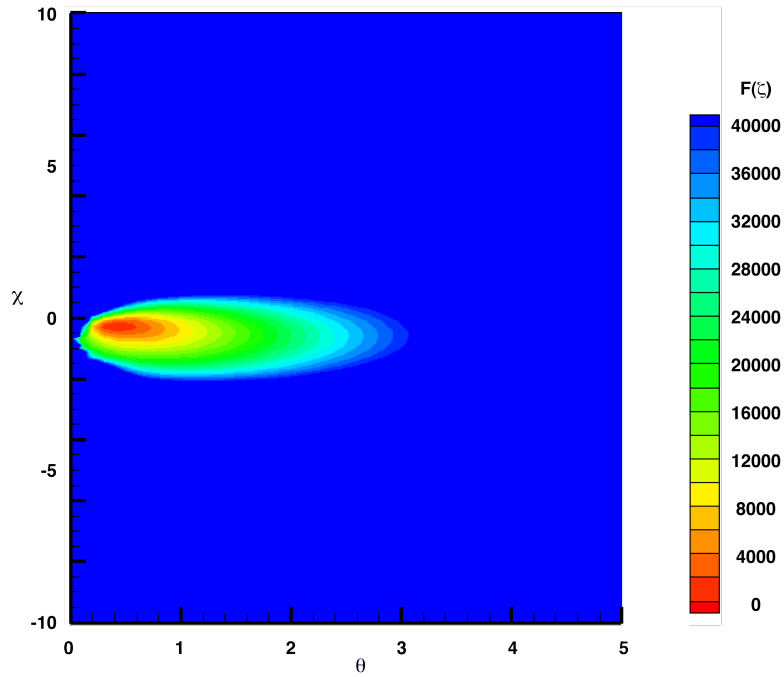
Of course, it is also possible to use contour maps of the cost function to determine the liner impedance. In this approach, the finite element method is used to compute the cost function for a range of liner impedances, from which the true liner impedance (that which causes the cost function to be minimized) is inferred. An example of results achieved with this contour map approach is presented in Figure 33 [57]. The eye of the contour is observed to be very diffuse (shallow gradients) for the 0.4 kHz data, which indicates there is a wide range of impedances for which the cost function is relatively constant. For this case, the SDFP optimizer is more prone to experience spurious results, where the search algorithm gets stuck in local optima. Conversely, the eye of the contour for the 1.8 kHz data is very sharp (steep gradients), and the SDFP optimizer is less prone to experience spurious results. The contour maps of Figure 33 are based on computations for $0 \leq \theta \leq 10$ and $-10 \leq \chi \leq 10$, with increments of 0.1 in both components (over 20,000 combinations), which is very computationally expensive. As a result, the contour map approach is only used when a detailed evaluation is required.

More recent implementations of the CHE method (sometimes labeled as Python CHE or PyCHE) support the use of a variety of optimizers contained within the SciPy optimization toolkit [58]. Previous studies [59] have considered three optimizers with this method. The first is a gradient-based optimizer based on sequential least squares programming (SLSQP), which provides similar results to those achieved with the SDFP algorithm. As with the SDFP, the use of a gradient-based optimizer necessitates multiple computations (i.e., separate eductions using multiple initial estimates of the liner impedance) in order to ensure that the optimum impedance is educed. In an attempt to alleviate the need for multiple computations, two global optimizers (Basin-Hopping and Differential Evolution algorithms) have been considered that are stochastic in nature and attempt to find the global minimum of a multivariate function. Both optimizers provide good results. The Differential Evolution is more efficient than the Basin-Hopping (as implemented), but still takes considerably more time than the SLSQP.

The CHE (and PyCHE) method of impedance eduction is heavily used by the NASA Liner Physics Team, as it directly accounts for the reflections that occur at the leading and trailing edges of the liner and at the duct termination. As such, it is easily extended to allow for multizone liners (multiple distinct axial zones).



(a) Shallow eye; 0.4 kHz.



(b) Sharp eye; 1.8 kHz.

Figure 33: Contour maps of $F(\zeta)$ as a function of normalized acoustic resistance and reactance.

4.3.2 Method Based on the Linearized Euler Equations (LEE)

The LEE method [54,60], based on a finite element solution to the linearized Euler equations (LEE), is suitable for those cases where the effects of one-dimensional shear flow in the vertical direction (from the lower rigid wall to the liner in the upper wall) are included. Equations for the linearized conservation of mass, axial momentum, and transverse momentum in a parallel, shear flow are given by

$$ikp + M \frac{\partial p}{\partial x} = -\rho c \left(\frac{\partial u}{\partial x} + \frac{\partial v}{\partial y} \right), \quad (20)$$

$$iku + M \frac{\partial u}{\partial x} + \frac{dM}{dy} v = -\frac{1}{\rho c} \frac{\partial p}{\partial x}, \quad (21)$$

$$ikv + M \frac{\partial v}{\partial x} = -\frac{1}{\rho c} \frac{\partial p}{\partial y}, \quad (22)$$

where homentropic flow is assumed (i.e., $p = \rho c^2$) and only plane waves are present in the spanwise (z) direction. Clearly, the linearized Euler equations can also be used with uniform flow. However, since the convected Helmholtz equation is simpler, most uniform-flow analysis conducted at NASA uses the CHE method.

If only plane waves are present in the hardwall sections upstream and downstream of the liner, the source and exit plane acoustic pressure boundary conditions are given by Equation (18), and the transverse acoustic particle velocity at the source plane is given by

$$v(0, y) = 0. \quad (23)$$

For this case, the wall impedance boundary condition proposed by Myers [53] is given by

$$v(x, H) = \left(1 + \frac{M(H)}{ik} \frac{\partial}{\partial x} \right) \left[\frac{p(x, H)}{\rho c \zeta} \right]. \quad (24)$$

As with the CHE, an optimizer is employed to find the impedance for which the predicted and measured acoustic pressures are matched to within an acceptable tolerance, i.e., the impedance that causes the objective function (Eq. (19)) to be minimized. Therefore, the LEE is also classified as an indirect method.

4.3.3 Method Based on the Pridmore-Brown Equation (PBE)

The first direct method to be considered is based on the solution to the Pridmore-Brown equation (PBE) [61,62]. Figure 32 shows a schematic of the duct. It is assumed that the duct is rectangular with height H and width W and that the two sidewalls are rigid. It is also assumed that the liner is mounted in the upper wall of the duct, and the flow is parallel (i.e., the flow velocity has a component only along the duct axis and its value is independent of the axial coordinate, x). Under these conditions, the acoustic pressure field in the liner region can be expressed in the form

$$p(x, y, z) = \sum_{m=0}^{\infty} \sum_{n=0}^{\infty} A_{mn} P_{mn}(y) e^{-iK_{mn}x} \cos \frac{m\pi z}{W}. \quad (25)$$

In this situation, the linearized equations that govern conservation of mass and momentum in the lined region of the duct can be combined into a single ordinary differential equation on the acoustic pressure eigenfunction, $P_{mn}(y)$, as

$$P''_{mn}(y) + \left[\frac{2k_{mn}M'(y)}{k - k_{mn}M(y)} \right] P'_{mn}(y) + \left[(k - k_{mn}M(y))^2 - k_{mn}^2 - \left(\frac{n\pi}{H} \right)^2 \right] P_{mn}(y) = 0. \quad (26)$$

Here, the axial wavenumbers, K_{mn} , with positive and negative imaginary parts correspond to right and left running duct modes, respectively. The wall boundary conditions are given by

$$P'_{mn}(0) = 0 \quad (27)$$

$$P'_{mn}(H) = -ik \left(1 - \frac{K_{mn}M(H)}{k} \right)^2 \frac{P_{mn}(H)}{\zeta} \quad (28)$$

where Equation (27) specifies a rigid lower wall and Equation (28) specifies an acoustic liner in the upper wall based on the Myers boundary condition.

If the axial wavenumbers (i.e., K_{mn}) are known, one can use the following procedure to determine the impedance of the liner mounted in the upper wall. First, the acoustic pressure eigenfunction, $P_{mn}(y)$, at the lower wall can only be determined to within an arbitrary multiplicative constant so its value is set to unity at the lower wall ($P_{mn}(0) = 1$). Next, the Pridmore-Brown equation (Eq. (26)) is integrated from the lower to the upper wall to determine $P_{mn}(H)$ and $P'_{mn}(H)$ at the upper wall (where the liner is located). Finally, the boundary condition at the upper wall (Eq. (28)) is used to compute the liner impedance. Given the efficiency of this approach, the PBE method is generally the preferred option at NASA for investigation of 1D shear flow effects on acoustic impedance. As an aside, an older paper by Parrott [63] and the recent article by Rienstra [64] are recommended for those interested in more detailed studies based on the 2D or 3D axisymmetric Pridmore-Brown equation.

Axial Wavenumber Determination The axial wavenumber determination is approached differently depending on whether the measured acoustic pressure field contains a dominant mode, or is contaminated with other modes that carry significant acoustic energy. Both cases are described in some detail below.

Single Mode Dominant As noted above, the PBE method requires the axial wavenumbers to be known. For application with data acquired in the GFIT, the frequency is kept sufficiently low so that only the plane wave mode ($m = 0$) is cut on in the horizontal (z) dimension. The acoustic pressure field (see Eq. (25)) can be rewritten as

$$p(x, y) = \sum_{n=0}^{\infty} A_{0n} P_{0n}(y) e^{-iK_{0n}x} \quad (29)$$

Note that there may be multiple modes present in the vertical (y) dimension. If one of these vertical modes is dominant, then the acoustic pressure field along the hardwall opposite the liner ($y = 0$) at measurement location x_j can be expressed in terms of this single dominant mode (n) as

$$p(x_j, 0) = A_{0n} P_{0n}(0) e^{-iK_{0n}x_j} = p_{ref} 10^{\text{SPL}(x_j)/20} e^{-i\phi(x_j)} \quad (30)$$

where the reference pressure, p_{ref} , is 20 μPa . In this situation, the axial SPL and phase profiles will decay monotonically along the length of the duct in our selected time convention ($e^{i\omega t}$). When this is observed in the data, the axial wavenumber is given by

$$K_{0n} = \frac{d\phi(x)}{dx} + \frac{i}{20\text{Log}_{10}(e)} \frac{d\text{SPL}(x)}{dx}. \quad (31)$$

In reality, the GFIT has a finite length and the acoustic liner forms only a portion of the wall of the GFIT (see Fig. 32). As a result, reflections occur at the impedance discontinuities at the leading and trailing edges of the liner and at the downstream termination of the GFIT. These reflections combine with the progressive sound field to cause standing waves over the axial extent of the liner. If these standing waves are sufficiently weak such that the axial decay remains predominantly monotonic, Equation (31) can be used with confidence. Indeed, this tends to be the case for the majority of acoustic liners that have been tested in the GFIT (as well as the earlier versions of this flow duct), regardless of the test condition (i.e., source SPL, frequency, and flow Mach number).

Multiple Modes Dominant When there is no single dominant mode, the Prony method [65] can be used to determine the axial wavenumber of a given mode [66,67]. If the acoustic pressure field is defined at an even number, q , of equally spaced points, $x = x_1, x = x_2, \dots, x_q$, on the lower wall of the flow duct, the prediction equations

$$[C] \{D\} = -\{G\} \quad (32)$$

can be constructed, where

$$[C] = \begin{bmatrix} p_2 & p_3 & p_4 & \cdots & p_{\eta+1} \\ p_3 & p_4 & p_5 & \cdots & p_{\eta+2} \\ p_4 & p_5 & p_6 & \cdots & p_{\eta+3} \\ p_5 & p_6 & p_7 & \cdots & p_{\eta+4} \\ \vdots & \vdots & \vdots & \vdots & \vdots \\ p_{q-\eta+1} & p_{q-\eta+2} & p_{q-\eta+3} & \cdots & p_q \end{bmatrix}, \{D\} = \begin{bmatrix} D_2 \\ D_3 \\ D_4 \\ \vdots \\ D_{\eta+1} \end{bmatrix}, \{G\} = \begin{bmatrix} p_1 \\ p_2 \\ p_3 \\ \vdots \\ p_\eta \end{bmatrix} \quad (33)$$

and p_1, p_2, \dots, p_q , are the measured values of $p(x, 0)$ at $x = x_1, x = x_2, \dots, x = x_q$, respectively, based on the microphone measurements, and η represents the number of modes included in the analysis. Note that the coefficients in the Hankel matrix, $[C]$, and right-hand-side vector, $\{G\}$, are known from the observed data set.

Singular value decomposition can then be used to obtain the generalized inverse of $[C]$

$$[C]^{-1} = [V][\Lambda]^{-1}[U^*]^T. \quad (34)$$

Here, $[U]$, $[V]$, $[\Lambda]$ are the matrices of left singular vectors, right singular vectors, and singular values, respectively. The singular value decomposition allows the normal and spurious (physical and non-physical) modes to be separated.

The generalized matrix inverse is then used to obtain the vector of polynomial coefficients, $\{D\}$

$$\{D\} = -[C]^{-1}\{G\} \quad (35)$$

and the linear prediction coefficients $D_2, D_3, \dots, D_{\eta+1}$ from the solution vector $\{D\}$ are used to construct the η^{th} degree polynomial,

$$\mathcal{F}(X) = 1 + D_2X + D_3X^2 + D_4X^3 + \dots, D_{\eta+1}X^\eta. \quad (36)$$

It can be shown that the zeros of $\mathcal{F}(X)$ are related to the axial propagation constants, K_{mn} , in the mode expansion in Eq. (29). However, some of these zeros are spurious and the axial wavenumber extracted from a spurious zero is not associated with a normal acoustic pressure mode.

The best solution is obtained when η equals the number of cut-on modes in the measured signal. However, the number of modes cannot be known a priori. Further, if η is chosen too small, there will be mode aliasing and the extracted axial wavenumbers, K_{0n} , will be perturbed from their true value. The best approach is therefore to choose η greater than the number of modes in the signal. Choosing η too large, however, has the disadvantage that extraneous solutions may be generated [66]. Therefore, if η is chosen larger than the number of normal modes in the duct, then a method of identifying the extraneous modes is needed.

Kumaresan and Tufts [68] provided a method for separating the zeros of $\mathcal{F}(X)$. First, a complex polynomial root finder is used to find the zeros, X , of the polynomial defined in Eq. (36). Next, the measured axial wavenumber, K_{0n} , is computed from the poles, s , of $\mathcal{F}(X)$

$$s = \frac{1}{X} = e^{i\Delta x K_{0n}} = \|s\|e^{i\Psi}. \quad (37)$$

The axial wavenumber is computed from these poles as

$$K_{0n} = \frac{\text{Log}_e [s]}{i\Delta x} \quad (38)$$

where Δx is the increment spacing between the q evenly spaced points. The axial wavenumbers corresponding to poles with a magnitude inside the unit circle (i.e., $\|s\| < 1$) are spurious while the remaining axial wave numbers (i.e., those for which $\|s\| \geq 1$) correspond to normal modes in the duct.

It should be noted that this algorithm for removing the spurious modes works very well for synthesized data, but is less robust when applied to data measured in the GFIT. This may be due to uncertainty in the measured acoustic pressures at each microphone location, but it remains as a limiting factor nonetheless. Thus, as a practical matter, there remains some engineering judgment required for determining which modes are appropriate for use in the impedance reduction analysis.

4.3.4 Single Mode Method (SMM)

The Single Mode Method [56, 69, 70] is a direct method based on the assumption that the flow is uniform and a single mode is dominant. Under these conditions, the SPL and phase axial profiles decay monotonically and Equation (31) can be used to determine the axial wavenumber. If a modal analysis is applied with the convected Helmholtz equation, the acoustic impedance (Myers boundary condition) of the liner mounted in the upper wall (at $y = H$) can be computed analytically as

$$\zeta = \frac{ik}{\lambda_{0n}} \left(1 - \frac{K_{0n}M}{k} \right)^2 \cot(\lambda_{0n}H), \quad (39)$$

where

$$\lambda_{0n}^2 = (k - K_{0n}M)^2 - K_{0n}^2. \quad (40)$$

As noted earlier, the SPL and phase axial profile decays measured in the GFIT have been observed to be predominantly monotonic for the vast majority of liners and test conditions. For this reason, the SMM has been used by the NASA Liner Physics Team for a number of years.

4.3.5 Prony Method (PM)

If the flow is uniform but a single mode is not dominant, the Prony Method is the current preferred method. The axial wavenumber is determined using Equations (32) - (38), and the liner impedance is determined using Equation (39).

The flexibility and ease of automation of the Prony Method make it the current tool of choice. The only drawback is that this method will occasionally select spurious modes (based on the selection of spurious axial wavenumbers), and will therefore provide anomalous results. Nevertheless, as the impedance of most liners is a relatively smooth function, it is generally rather simple to determine where these spurious modes occur. This engineering judgment requirement is not ideal, but is considered to be a reasonable compromise given the efficiency of the method. As a practical matter, a smoothing function can often be applied to the deduced impedance spectra to account for these anomalies.

4.3.6 In Situ Method (ISM)

The ISM described earlier (Sec. 4.2.1) is another direct method that has been implemented in the GFIT. This method allows for direct determination of the acoustic impedance based on Equation (6). The measurements are acquired with one microphone flush-mounted in the surface of the liner and the other flush-mounted in the backplate of the liner (see Fig. 34). Of particular interest is the fact that this method captures the effects of grazing flow implicitly, i.e., without the need for changes to the equation or the way in which the acoustic pressure data is acquired. This method is included here for completeness, but is very rarely employed at NASA due to the difficulties noted in Section 4.2.1.

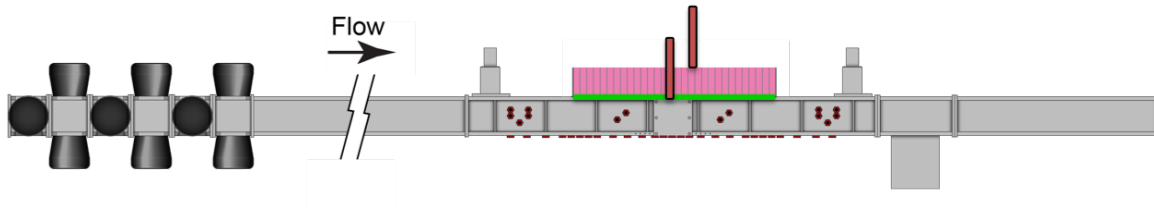


Figure 34: Sketch of GFIT with microphones embedded in liner for use with In Situ Method.

4.3.7 Hybrid Method

The CHE (or PyCHE) and Prony methods are the methods most commonly used at NASA for impedance eduction based on data acquired in the GFIT. The CHE is used because of its ability to account for reflections within the test section, while the Prony method is much faster than the CHE but cannot explicitly handle reflections in the test section.

As noted earlier, NASA is currently transitioning the source type from stepped-sine to swept-sine. Most tests in the GFIT have traditionally been conducted using a stepped-sine source at frequencies of 0.4 to 3.0 kHz in 0.2 kHz increments, for a total of 14 frequencies. The current version of the swept-sine source covers the same frequency range, but acquires data at 0.01 kHz increments, for a total of 261 frequencies. While these additional data are certainly helpful in the assessment of an acoustic liner, they also represent a significant increase in data analysis time. Thus, a more efficient impedance eduction method is needed in order to take full advantage of this new data acquisition approach.

A hybrid approach has been recently implemented to support this analysis. First, the Prony method is employed to get an initial estimate of the liner impedance. This result is then used as an initial estimate for the PyCHE, which employs the SLSQP gradient-based optimizer to determine the liner impedance. The likelihood is high that the correct answer is determined since the Prony answer is at or very near the correct answer (indeed, Prony results can often be used as the final answer). This hybrid approach avoids the need for multiple eductions with a gradient-based optimizer and is also much quicker than using global optimizers that require no initial estimate.

5 Additional Effects of Higher-Order Modes

Multiple tests have been conducted in the GFIT and CDTR to demonstrate the intrinsic nature of the acoustic impedance. For each test, two liners are fabricated with the same geometric parameters (core depth and facesheet hole diameter, porosity, and thickness), one sized to fit in the upper wall of the GFIT and the other sized to fit in the sidewall of the CDTR. Impedances educed with data acquired in the GFIT are then used as input to a propagation code to predict the effects of the liner on the sound field in the CDTR. As the CDTR can be operated with a number of selected modes (one at a time), favorable comparisons of the predicted and measured transmission losses provide strong evidence that the acoustic impedance is indeed an intrinsic parameter. Of course, a favorable comparison also suggests that the propagation code is valid.

One such evaluation was presented by Gerhold, et al. [71]. The CHE method was used with data acquired in the GFIT to determine the acoustic impedance of a conventional perforate-over-honeycomb liner. A similar liner was then tested in the CDTR for a number of selected modal sources. For each test condition, the acoustic pressure fields measured in the CDTR hardwall sections upstream and downstream of the acoustic liner were decomposed into their respective modal contents. For a selected mode ($\{0,2\}$ for the case shown in Figure 35; i.e., $m = 0, n = 2$), the upstream modal content (includes the modal coefficients for all propagating modes) and the liner impedance were used as input to the CDUCT-LaRC duct propagation code [72–74]. This code, based on a parabolic approximation to the convected Helmholtz equation, was used to compute the acoustic pressure field throughout the CDTR. A comparison of measured and predicted attenuation (transmission loss) spectra based on data acquired for the $\{0,2\}$ mode and Mach 0.275 flow (flow profile is assumed to be uniform) is provided in Figure 35. Although mode separation was not sufficient for some of the frequencies to support the computation, a favorable comparison is observed at the majority of test frequencies.

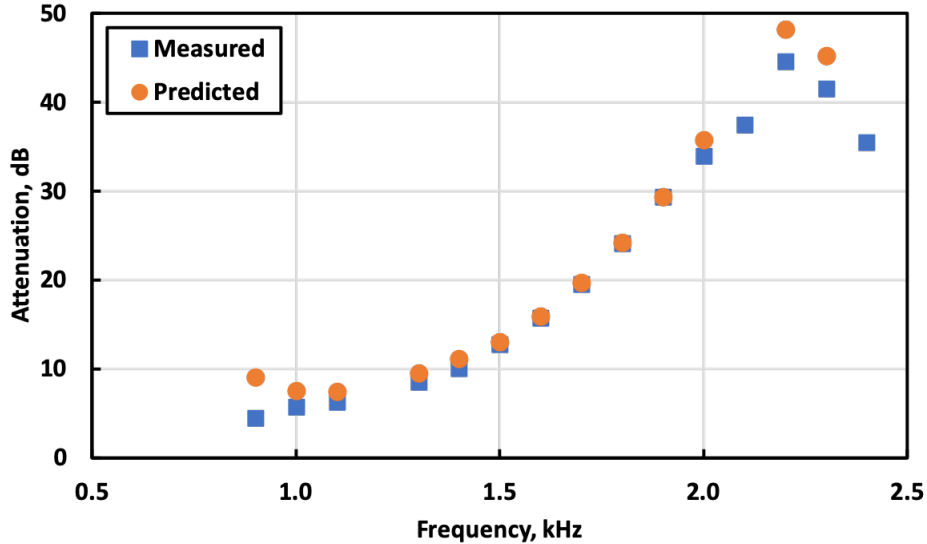


Figure 35: Comparison of measured and predicted attenuation for the $\{0,2\}$ mode at $M = 0.275$.

The acoustic impedance is presumed to be independent of the acoustic pressure mode to which the liner is subjected. Thus, an impedance educed in the GFIT can be used to predict the sound absorption when the same liner is mounted in an aircraft engine nacelle. One of the first demonstrations of this was provided by Watson, et al. [75]. The Prony method was used with GFIT data to educe the impedance of the test liner. A second liner with identical geometric parameters was mounted in the CDTR and the microphones in the upper wall of the treated section were used to determine the acoustic pressure field. Impedance spectra were educed for three distinct modes using the Prony method. The comparisons (see Figs. 36 and 37) are excellent over the majority of the frequency range. The result at 0.3 kHz for $n = 0$ appears anomalous, and may be due to the selection of a spurious mode in the Prony method. Discrepancies at the higher frequencies are likely due to the fact that the CDTR control system did not achieve sufficient separation between the desired mode ($\{0,0\}$, $\{0,1\}$, or $\{0,2\}$) and all other modes.⁵ Table 2 provides a list of modes and their corresponding cut on frequencies for Mach 0.3 flow in the CDTR. It includes all modes that cut on at frequencies below 3.0 kHz. At a frequency of 1.6 kHz, where the results in Figs. 36 and 37 begin to diverge, there are seven modes that are cut on at Mach 0.3. Thus, the control system is attempting to reduce the energy in the six undesired modes. At 2.5 kHz, the number of undesired modes that are cut on has doubled to twelve, significantly increasing the difficulty of achieving mode separation.

Regardless, the excellent agreement over the frequency range where the control system is able to achieve separation between the desired mode and all other cut on modes demonstrates that the acoustic impedance is independent of the mode to which the liner is subjected. This provides further proof that the acoustic impedance is an intrinsic parameter. These results also demonstrate that

⁵These results were acquired when the CDTR had 16 drivers, reducing the frequency range for which significant mode separation could be achieved.

impedance eduction based on excitation of higher-order modes is more difficult than for the $\{0,0\}$ mode.

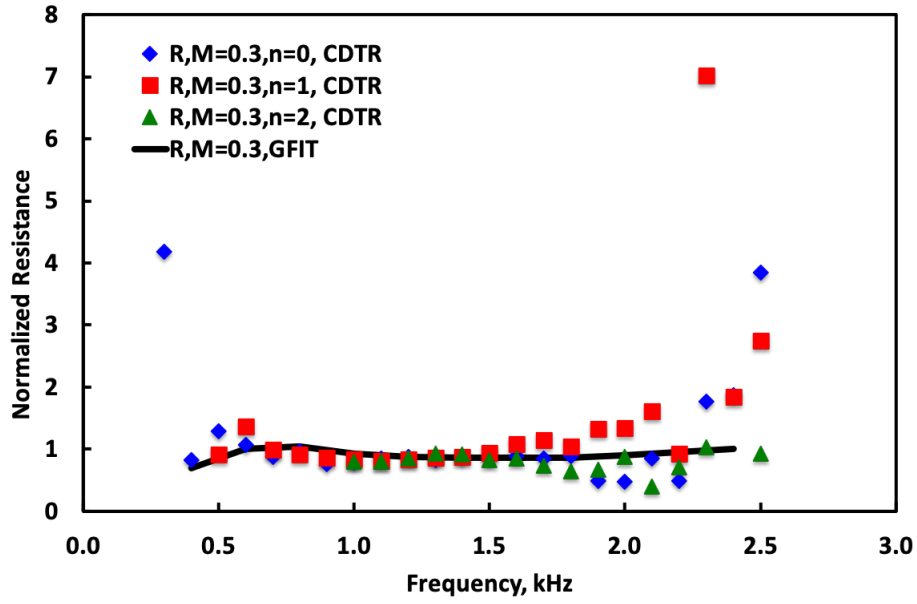


Figure 36: Comparison of resistance spectra educed in the GFIT and CDTR ($m = 0$).

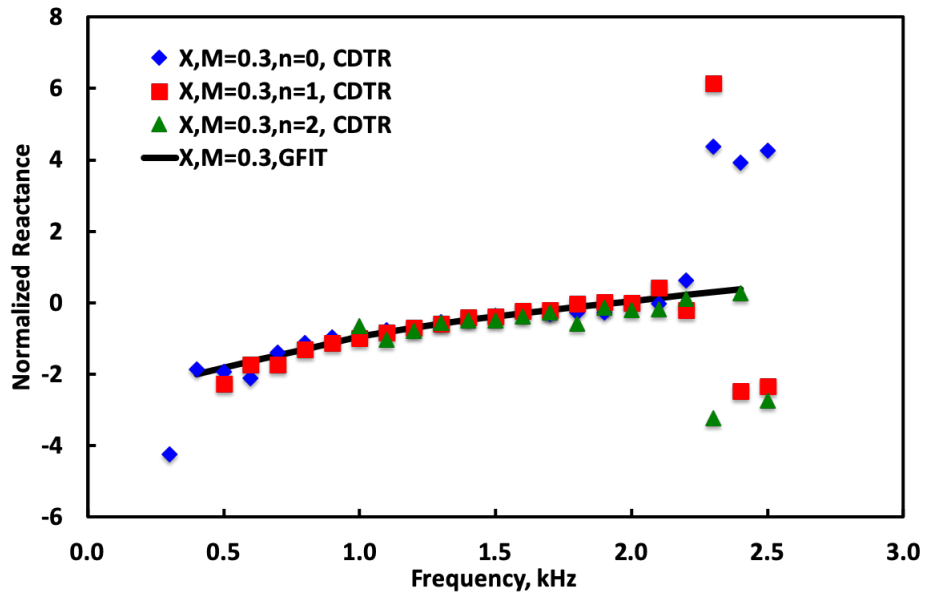


Figure 37: Comparison of reactance spectra educed in the GFIT and CDTR ($m = 0$).

6 Concluding Remarks

This report has provided a technical overview of acoustic liner research conducted at the NASA Langley Research Center over the last four decades. Specifically, it has highlighted a number of test rigs, past and present, that have been used to determine the acoustic impedance for conventional and novel liners. Descriptions of the operational domains for the current test rigs were also presented, as well as a number of methods to investigate the effects of frequency, source sound pressure level, source type, flow Mach number, and higher-order modes.

Table 2: Cut-on frequencies for modes in the CDTR at Mach 0.3.

Freq, kHz	Mode {m,n}	Freq, kHz	Mode {m,n}	Freq, kHz	Mode {m,n}
0.000	{0,0}	1.382	{1,2}	2.201	{2,1}
0.432	{0,1}	1.686	{1,3}	2.325	{2,2}
0.863	{0,2}	1.727	{0,4}	2.413	{1,5}
1.079	{1,0}	2.036	{1,4}	2.517	{2,3}
1.162	{1,1}	2.158	{0,5}	2.764	{2,4}
1.295	{0,3}	2.158	{2,0}		

References

1. Ingard, U., "On the Theory and Design of Acoustic Resonators," *Journal of the Acoustical Society of America*, Vol. 25, 1953, pp. 1037–1061.
2. Khorrami, M. R., Humphreys, Jr., W. M., Lockard, D. P., and Ravetta, P. A., "Aeroacoustic Evaluation of Flap and Landing Gear Noise Reduction Concepts," AIAA Paper 2014-2478, June 2014.
3. Jones, M. G. and Howerton, B. M., "Evaluation of Novel Liner Concepts for Fan and Airframe Noise Reduction," AIAA Paper 2016-2787, May 2016.
4. Blackstock, D. T., *Fundamentals of Physical Acoustics*, Wiley, 2000.
5. Jones, M. G., Howerton, B. M., and Ayle, E., "Evaluation of Parallel-Element, Variable-Impedance, Broadband Acoustic Liner Concepts," AIAA Paper 2012-2194, June 2012.
6. Nark, D. M. and Jones, M. G., "Broadband Liner Optimization for the Source Diagnostic Test Fan," AIAA Paper 2012-2195, June 2012.
7. Nark, D. M., Jones, M. G., and Sutliff, D. L., "Further Development and Assessment of a Broadband Liner Optimization Process," AIAA Paper 2016-2784, May 2016.

8. Jones, M. G., Nark, D. M., Baca, A., and Smith, C. R., "Applications of Parallel-Element, Embedded Mesh-Cap, Acoustic Liner Concepts," AIAA Paper 2018-3445, June 2018.
9. Nark, D. M., Jones, M. G., Schiller, N. H., and Sutliff, D. L., "Broadband Inlet Liner Design for the DGEN Aeropropulsion Research Turbofan," AIAA Paper 2018-3608, June 2018.
10. Sutliff, D. L., Nark, D. M., Jones, M. G., and Schiller, N. H., "Design and Acoustic Efficacy of a Broadband Liner for the Inlet of the DGEN Aero-propulsion Research Turbofan," AIAA Paper 2019-2582, May 2019.
11. Nark, D. M. and Jones, M. G., "Design of an Advanced Inlet Liner for the Quiet Technology Demonstrator 3," AIAA Paper 2019-2764, May 2019.
12. Wong, J. W., Nesbitt, E. H., Jones, M. G., and Nark, D. M., "Flight Test Methodology for NASA Advanced Inlet Liner on 737MAX-7 Test Bed (Quiet Technology Demonstrator 3)," AIAA Paper 2019-2763, May 2019.
13. Sutliff, D. L., Jones, M. G., and Hartley, T. C., "High-Speed Turbofan Noise Reduction Using Foam-Metal Liner Over-the-Rotor," *Journal of Aircraft*, Vol. 50, No. 5, September-October 2013, pp. 1491–1503.
14. Brown, M. C., Jones, M. G., Howerton, B. M., Syed, A., Shafer, L., Ichihashi, F., and Bowen, L., "Flow Resistance Comparative Study," NASA TM 220262, March 2019.
15. Howerton, B. M., Vold, H., and Jones, M. G., "Application of Sine Sweep Excitation for Acoustic Impedance Education," AIAA Paper 2019-2487, May 2019.
16. Watson, W. R., Jones, M. G., Tanner, S. E., and Parrott, T. L., "Validation of a Numerical Method for Extracting Liner Impedance," *AIAA Journal*, Vol. 34, No. 3, 1996, pp. 548–554.
17. Jones, M. G., Watson, W. R., Parrott, T. L., and Smith, C. D., "Design and Evaluation of Modifications to the NASA Langley Flow Impedance Tube," AIAA Paper 2004-2837, May 2004.
18. Renou, Y. and Auregan, Y., "Failure of the Ingard-Myers Boundary Condition for a Lined Duct: An Experimental Investigation," *Journal of the Acoustical Society of America*, Vol. 130, No. 1, July 2011, pp. 52–60.
19. Eversman, W. and Gallman, J. M., "Impedance Education with an Extended Search Procedure," *AIAA Journal*, Vol. 49, No. 9, September 2011, pp. 1960–1970.
20. Watson, W. R. and Jones, M. G., "Evaluation of Wall Boundary Conditions for Impedance Education Using a Dual-Source Method," AIAA Paper 2012-2199, June 2012.
21. Zhou, L., Boden, H., Lahiri, C., Bake, F., Enghardt, L., Busse-Gerstengarbe, S., and Elnady, T., "Comparison of impedance education results using different methods and test rigs," AIAA Paper 2014-2955, June 2014.
22. Zhou, L. and Boden, H., "A systematic uncertainty analysis for liner impedance education technology," *Journal of Sound and Vibration*, Vol. 356, 2015, pp. 86–99.

23. Schulz, A., Weng, C., Bake, F., Enghardt, L., and Ronneberger, D., "Modeling of liner impedance with grazing shear flow using a new momentum transfer boundary condition," AIAA Paper 2017-3377, June 2017.
24. Nark, D. M., Jones, M. G., and Piot, E., "Assessment of Axial Wavenumber and Mean Flow Uncertainty on Acoustic Liner Impedance Education," AIAA Paper 2018-3444, June 2018.
25. Roncen, R., Piot, E., Mery, F., Simon, F., Jones, M. G., and Nark, D. M., "Influence of Source Propagation Direction and Shear Flow Profile in Impedance Education of Acoustic Liners," AIAA Paper 2019-2469, May 2019.
26. Jones, M. G., Watson, W. R., Howerton, B. M., and Busse-Gerstengarbe, S., "Effects of Mean Flow Assumption and Harmonic Distortion on Impedance Education Methods," *AIAA Journal*, Vol. 53, No. 6, June 2015, pp. 1503–1514.
27. Parrott, T. L. and Jones, M. G., "Assessment of NASA's Aircraft Noise Prediction Capability, Chapter 6: Uncertainty in Acoustic Liner Impedance Measurement and Prediction," NASA TP 2012-215653, July 2012.
28. Watson, W. R. and Nark, D. M., "Assessment of NASA's Aircraft Noise Prediction Capability, Chapter 6: Assessment of Acoustic Propagation and Radiation Codes for Locally Reacting Liners in Flow Ducts," NASA TP 2012-215653, July 2012.
29. Howerton, B. M. and Jones, M. G., "Acoustic Liner Drag: A Parametric Study of Conventional Configurations," AIAA Paper 2015-2230, June 2015.
30. Howerton, B. M. and Jones, M. G., "A Conventional Liner Acoustic/ Drag Interaction Benchmark Database," AIAA Paper 2017-4190, June 2017.
31. Howerton, B. M., Jones, M. G., and Jasinski, C. M., "Acoustic Liner Drag: Further Measurements on Novel Facesheet Perforate Geometries," AIAA Paper 2018-3605, June 2018.
32. Mery, F., Conte, C., Leon, O., and Piot, E., "Non-intrusive measurements of velocity fields over a lined wall in a turbulent duct flow for drag assessment," AIAA Paper 2017-3025, June 2017.
33. Gerhold, C. H., Brown, M. C., Jones, M. G., and Howerton, B. M., "Report on Recent Upgrades to the Curved Duct Test Rig at NASA Langley Research Center," AIAA Paper 2011-2896, June 2011.
34. Gerhold, C. H., Brown, M. C., Jones, M. G., and Howerton, B. M., "Configuration Effects on Liner Performance," AIAA Paper 2012-2245, June 2012.
35. Gerhold, C. H., Brown, M. C., Jones, M. G., Nark, D., and Howerton, B. M., "Configuration Effects on Acoustic Performance of a Duct Liner," AIAA Paper 2008-2977, May 2008.
36. Gerhold, C. H., Brown, M. C., and Jasinski, C. M., "Evaluation of Skin Friction Drag for Liner Applications in Aircraft," AIAA Paper 2016-1267, January 2016.
37. Syed, A. A., Yu, J., Kwan, H. W., and Chien, E., "The Steady Flow Resistance of Perforated Sheet Materials in High Speed Grazing Flows," NASA CR 2002-211749, 2002.

38. Motsinger, R. E. and Kraft, R. E., "Design and Performance of Duct Acoustic Treatment: Aeroacoustics of Flight Vehicles; Chapter 14, Vol. 2: Noise Control," NASA RP 1258, August 1991.
39. Simon, F., Marchner, P., Romcen, R., and Chevillotte, F., "Comportement d'un liner acoustique par approche de type Lattice Boltzmann," Cfa 2018 - le havre, April 2018.
40. Parrott, T. L. and Jones, M. G., "Parallel-Element Liner Impedances for Improved Absorption of Broadband Sound in Ducts," *Noise Control Engineering Journal*, Vol. 43, No. 6, November - December, 1995.
41. Dean, P. D., "An In Situ Method Of Wall Acoustic Impedance Measurement In Flow Ducts," *Journal of Sound and Vibration*, Vol. 34, No. 1, 1974, pp. 97–130.
42. Zandbergen, T., "On the practical use of a three-microphone technique for in-situ acoustic impedance measurements on double layer flow duct liners," AIAA Paper 1981-2000, 1981.
43. Murray, P. B., Ferrante, P., and Scofano, A., "Manufacturing process and boundary layer influences on perforate liner impedances," AIAA Paper 2005-2849, May 2005.
44. Gaeta, R. J., Mendoza, J. M., and Jones, M. G., "Implementation of In-Situ Impedance Techniques on a Full Scale Aero-Engine System," AIAA Paper 2007-3441, May 2007.
45. Beranek, L. L., *Acoustical Measurements (revised edition)*, American Institute of Physics, Woodbury, NY, 1988.
46. Kinsler, L. E. and Frey, A. R., *Fundamentals of Acoustics*, John Wiley & Sons, Second Edition, 1962.
47. Parrott, T. L. and Smith, C. D., "Random and Systematic Measurement Errors in Acoustic Impedance as Determined by the Transmission Line Method," NASA TN D 8520, December 1977.
48. Jones, M. G. and Parrott, T. L., "Evaluation of a multi-point method for determining acoustic impedance," *Journal of Mechanical Systems and Signal Processing*, Vol. 3, No. 1, 1989, pp. 15–35.
49. Jones, M. G. and Stiede, P. E., "Comparison of Methods for Determining Specific Acoustic Impedance," *Journal of the Acoustical Society of America*, Vol. 101, No. 5, May 1997, pp. 2694–2704.
50. Ingard, U. and Singhal, V. K., "Sound attenuation in turbulent pipe flow," *Journal of the Acoustical Society of America*, Vol. 55, 1974, pp. 535–538.
51. Chung, J. Y. and Blaser, D. A., "Transfer function method of measuring in-duct acoustic properties: I. Theory," *Journal of Acoustical Society of America*, Vol. 68, 1980, pp. 907–921.
52. Tyler, J. and Sofrin, T., "Axial flow compressor noise studies," *Transactions of the Society of Automotive Engineers*, Vol. 70, 1962, pp. 309–332.

53. Myers, M. K., "On the Acoustic Boundary Condition in the Presence of Flow," *Journal of Sound and Vibration*, Vol. 71, No. 3, 1980, pp. 429–434.
54. Watson, W. R. and Jones, M. G., "Impedance Eduction in a Duct Using the Linearized Euler Equations," AIAA Paper 2018-3442, June 2018.
55. Stewart III, G. W., "A Modification of Davidon's Minimization Method to Accept Difference Approximations of Derivatives," *Journal of ACM*, Vol. 14, No. 1, 1967, pp. 72–83.
56. Watson, W. R. and Jones, M. G., "A Comparative Study of Four Impedance Eduction Methodologies Using Several Test Liners," AIAA Paper 2013-2274, May 2013.
57. Jones, M. G. and Watson, W. R., "Validation of an Improved Experimental Method for Use in Impedance Eduction," *AIAA Journal*, Vol. 51, No. 1, January 2013, pp. 186–199.
58. Jones, E., Oliphant, T., Peterson, P., et al., "SciPy: Open source scientific tools for Python," URL: <http://www.scipy.org/>, 2001–.
59. Jones, M. G., Watson, W. R., Nark, D. M., and Howerton, B. M., "Impedance Eduction for Multisegment Liners," AIAA Paper 2018-3441, June 2018.
60. Watson, W. R. and Jones, M. G., "Comparison of Convected Helmholtz and Euler Model for Impedance Eduction in Flow," AIAA Paper 2006-2643, May 2006.
61. Pridmore-Brown, D. C., "Sound Propagation in a Fluid Flowing Through an Attenuating Duct," *Journal of Fluid Mechanics*, Vol. 4, 1958, pp. 393–406.
62. Mungur, P. and Gladwell, G. M. L., "Acoustic Wave Propagation in a Sheared Fluid Contained in a Duct," *Journal of Sound and Vibration*, Vol. 9, No. 1, 1969, pp. 28–48.
63. Parrott, T. L., Watson, W. R., and Jones, M. G., "Experimental Validation of a Two-Dimensional Shear-Flow Model for Determining Acoustic Impedance," NASA TP 2679, May 1987.
64. Rienstra, S. W., "Solutions and Properties of the Pridmore-Brown Equation," AIAA Paper 2019-2594, May 2019.
65. de Prony, R., "Essai Éxperimental et Analytique: Sur Les Lois de la Dilatabilité de Fluides Élastique et sur Celles de la Force Expansive de la Vapeur de L'alkool, À différentes Temperatures," *Journal de l'école Polytechnique*, Vol. 1, No. 22, 1795, pp. 24–76.
66. Watson, W. R., Carpenter, M. H., and Jones, M. G., "Performance of Kumaresan and Tufts Algorithm in Liner Impedance Eduction with Flow," *AIAA Journal*, Vol. 53, No. 4, April 2015, pp. 1091–1102.
67. Jones, M. G., Watson, W. R., and June, J. C., "Optimization of Microphone Locations for Acoustic Liner Impedance Eduction," AIAA Paper 2015-3271, June 2015.
68. Kumaresan, R. and Tufts, D., "Estimating the Parameters of Exponentially Damped Sinusoids and Pole-Zero Modeling in Noise," *IEEE Transactions on Acoustics, Speech, and Signal Processing*, Vol. 30, No. 6, December 1982, pp. 833–840.

69. Armstrong, D. L., Beckemeyer, R. J., and Olsen, R. F., "Impedance Measurements of Acoustic Duct Liners With Grazing Flow," Paper presented at 87th Meeting of the Acoustical Society of America 1999-1864, 1974.
70. Jones, M. G., Watson, W. R., Tracy, M. B., and Parrott, T. L., "Comparison of Two Waveguide Methods for Educing Liner Impedances in Grazing Flow," *AIAA Journal*, Vol. 42, No. 2, February 2004, pp. 232–240.
71. Gerhold, C. H., Jones, M. G., Brown, M. C., and Nark, D., "Advanced computational and experimental techniques for nacelle liner performance evaluation," AIAA Paper 2009-3168, May 2009.
72. Nark, D. M., Farassat, F., Pope, D. S., and Vatsa, V., "The Development of the Ducted Fan Noise Propagation and Radiation Code CDUCT-LARC," AIAA Paper 2003-3242, May 2003.
73. Nark, D. M., Watson, W. R., and Jones, M. G., "An Investigation of Two Acoustic Propagation Codes for Three-Dimensional Geometries," AIAA Paper 2005-3022, May 2005.
74. Nark, D. M. and Farassat, F., "CDUCT-LaRC Status - Shear Layer Refraction and Noise Radiation," AIAA Paper 2006-2587, 2006.
75. Watson, W. R., Gerhold, C. H., Jones, M. G., and June, J. C., "Single Mode Theory for Impedance Education in Large-Scale Ducts with Grazing Flow," AIAA Paper 2014-3351, June 2014.

REPORT DOCUMENTATION PAGE

Form Approved
OMB No. 0704-0188

The public reporting burden for this collection of information is estimated to average 1 hour per response, including the time for reviewing instructions, searching existing data sources, gathering and maintaining the data needed, and completing and reviewing the collection of information. Send comments regarding this burden estimate or any other aspect of this collection of information, including suggestions for reducing this burden, to Department of Defense, Washington Headquarters Services, Directorate for Information Operations and Reports (0704-0188), 1215 Jefferson Davis Highway, Suite 1204, Arlington, VA 22202-4302. Respondents should be aware that notwithstanding any other provision of law, no person shall be subject to any penalty for failing to comply with a collection of information if it does not display a currently valid OMB control number.
PLEASE DO NOT RETURN YOUR FORM TO THE ABOVE ADDRESS.

1. REPORT DATE (DD-MM-YYYY) 01-04-2020		2. REPORT TYPE Technical Publication		3. DATES COVERED (From - To)	
4. TITLE AND SUBTITLE A Review of Acoustic Liner Experimental Characterization at NASA Langley				5a. CONTRACT NUMBER	
				5b. GRANT NUMBER	
				5c. PROGRAM ELEMENT NUMBER	
6. AUTHOR(S) Michael G. Jones, Willie R. Watson, Douglas M. Nark, Brian M. Howerton, and Martha C. Brown <i>NASA Langley Research Center, Hampton, VA 23681</i>				5d. PROJECT NUMBER	
				5e. TASK NUMBER	
				5f. WORK UNIT NUMBER 081876.02.07.12.01.02	
7. PERFORMING ORGANIZATION NAME(S) AND ADDRESS(ES) NASA Langley Research Center Hampton, Virginia 23681-2199				8. PERFORMING ORGANIZATION REPORT NUMBER L-21137	
9. SPONSORING/MONITORING AGENCY NAME(S) AND ADDRESS(ES) National Aeronautics and Space Administration Washington, DC 20546-0001				10. SPONSOR/MONITOR'S ACRONYM(S) NASA	
				11. SPONSOR/MONITOR'S REPORT NUMBER(S) NASA/TP-2020-220583	
12. DISTRIBUTION/AVAILABILITY STATEMENT Unclassified-Unlimited Subject Category 71 Availability: NASA STI Program (757) 864-9658					
13. SUPPLEMENTARY NOTES An electronic version can be found at http://ntrs.nasa.gov .					
14. ABSTRACT This paper presents a review of tools used by the NASA Langley Research Center over the last four decades to experimentally characterize acoustic liners for aircraft noise reduction. Descriptions of past and present NASA test rigs are included to provide context for the application of data acquisition and analysis methods. These test rigs range from simple applications of a raylometer to a waveguide with detailed control over higher-order modes. Methods for impedance reduction based on data acquired in these test rigs are explored in some detail. Strengths and weaknesses of each data acquisition and analysis method are presented, as well as current practices applied in the NASA Langley Liner Technology Facility.					
15. SUBJECT TERMS acoustic, liner, impedance, eduction					
16. SECURITY CLASSIFICATION OF:			17. LIMITATION OF ABSTRACT	18. NUMBER OF PAGES	19a. NAME OF RESPONSIBLE PERSON
a. REPORT	b. ABSTRACT	c. THIS PAGE			STI Information Desk (help@sti.nasa.gov)
U	U	U	UU	57	19b. TELEPHONE NUMBER (Include area code) (757) 864-9658